

**Special Collection:**  
Prediction in coastal  
geomorphology

#### Key Points:

- We propose a quantitative ternary diagram of delta morphology to compare predictions with observations
- Among 31 global deltas, the prediction error is lowest if there is a single dominant forcing compared with mixed-influenced deltas
- The quantitative ternary framework bridges the gap between natural and modeled deltas to predict and hindcast delta morphology

#### Correspondence to:

J. F. Paniagua-Arroyave,  
[jpaniag2@eafit.edu.co](mailto:jpaniag2@eafit.edu.co);  
[juan.paniaguaarroyave@colorado.edu](mailto:juan.paniaguaarroyave@colorado.edu)

#### Citation:

Paniagua-Arroyave, J. F., & Nienhuis, J. H. (2024). The quantified Galloway ternary diagram of delta morphology. *Journal of Geophysical Research: Earth Surface*, 129, e2024JF007878. <https://doi.org/10.1029/2024JF007878>

Received 20 JUN 2024

Accepted 22 OCT 2024



#### Author Contributions:

**Conceptualization:** Juan F. Paniagua-Arroyave, Jaap H. Nienhuis  
**Data curation:** Juan F. Paniagua-Arroyave, Jaap H. Nienhuis  
**Formal analysis:** Juan F. Paniagua-Arroyave, Jaap H. Nienhuis  
**Funding acquisition:** Jaap H. Nienhuis  
**Investigation:** Juan F. Paniagua-Arroyave, Jaap H. Nienhuis  
**Methodology:** Juan F. Paniagua-Arroyave, Jaap H. Nienhuis  
**Project administration:** Jaap H. Nienhuis  
**Resources:** Juan F. Paniagua-Arroyave, Jaap H. Nienhuis  
**Software:** Juan F. Paniagua-Arroyave, Jaap H. Nienhuis  
**Supervision:** Jaap H. Nienhuis

© 2024 The Author(s).

This is an open access article under the terms of the [Creative Commons Attribution-NonCommercial License](#), which permits use, distribution and reproduction in any medium, provided the original work is properly cited and is not used for commercial purposes.

# The Quantified Galloway Ternary Diagram of Delta Morphology

Juan F. Paniagua-Arroyave<sup>1,2,3</sup>  and Jaap H. Nienhuis<sup>1</sup> 

<sup>1</sup>Department of Physical Geography, Faculty of Geosciences, Utrecht University, Utrecht, The Netherlands, <sup>2</sup>Area of Natural Systems and Sustainability, School of Applied Sciences and Engineering, EAFIT University, Medellin, Colombia,

<sup>3</sup>INSTAAR, University of Colorado Boulder, Boulder, CO, USA

**Abstract** Waves, rivers, and tides shape delta morphology. Recent studies have enabled predictions of their relative influence on deltas globally, but methods and associated uncertainties remain poorly known. Here, we address that gap and show how to quantify delta morphology within the Galloway ternary diagram of river, wave, and tidal sediment fluxes. We assess delta morphology predictions compared to observations for 31 deltas globally and find a median error of 4% (standard deviation of 11%) in the river, tide, or wave-driven sediment fluxes. Relative uncertainties are greatest for mixed-process deltas (e.g., Sinu, error of 49%) and tend to decrease for end-member morphologies where either wave, tide, or river sediment fluxes dominate (e.g., Fly, error of 0.2%). Prediction uncertainties for delta morphologic metrics are more considerable: the delta shoreline protrusion angles set by wave influence have a median error of 45%, the delta channel widening from tides 25%, and the number of distributary channels 86%. Larger sources of prediction uncertainty are (a) delta morphology data, for example, delta slopes that modulate tidal fluxes, (b) data on river sediment flux distribution between individual delta river outlets, and (c) theoretical basis behind fluvial and tidal dominance. Broadly, these methods will help improve delta morphology predictions and assess how natural and anthropogenic forces affect morphologic change.

**Plain Language Summary** Waves, rivers, and tides determine the shape of river deltas, but it remains challenging to predict exactly how much. Recent studies have attempted to predict delta shape but fall short in quantifying the accuracy. Here, we propose a new method for predicting delta shape and assessing the predictions by looking at the pointiness of their shorelines, the number of river channels, and channel width. We apply our new approach to 31 deltas worldwide and find a median error of 4% with a maximum of 49% (Sinu delta) and a minimum of 0.2% (Fly delta). These methods can be used to predict future river delta changes and hindcast past delta shapes.

## 1. Introduction

The sustainable development of coastal communities depends upon our ability to predict future coastal morphological changes, particularly at deltas. Deltas exist at the confluence of marine and terrestrial sediment fluxes, which create highly dynamic land-ocean (coastal) environments and make predictions particularly challenging (Goodbred & Saito, 2012; Syvitski & Saito, 2007). To accurately predict delta morphology, we need a framework that couples both marine and terrestrial realms, as the balance between these forcings decisively controls the morphodynamics that dictates delta morphology (Caldwell et al., 2019; Fisher, 1969).

The earliest attempts at creating such a framework (Galloway, 1975) introduced a ternary diagram, which qualitatively distinguished the relative roles of wave, tide, and river fluxes on delta morphology. In Galloway's original triangle, delta morphology could be predicted based on the magnitudes of these processes by assigning a location within the triangle for a given fluvial discharge, wave power, and tidal power (e.g., Boyd et al., 1992). Later works expanded this method by employing numerical simulations and physical experiments exploring delta features' emergence from the effects of waves and tides (Baumgardner, 2016; Seybold et al., 2007).

Beyond the ternary diagram, statistical analyses of delta features (i.e., delta area, number of channels, delta gradient, and channel width) rendered predictive relationships helpful in assessing future environmental scenarios (Syvitski & Saito, 2007). However, a physical linkage between delta morphology and the balance between marine and terrestrial forces remained missing.

**Validation:** Juan F. Paniagua-Arroyave,  
Jaap H. Nienhuis

**Visualization:** Juan F. Paniagua-  
Arroyave, Jaap H. Nienhuis

**Writing – original draft:** Juan

F. Paniagua-Arroyave, Jaap H. Nienhuis

**Writing – review & editing:** Juan

F. Paniagua-Arroyave, Jaap H. Nienhuis

Here, we build on a recent contribution (Nienhuis et al., 2020) that reformulated Galloway's (1975) work into a quantitative ternary diagram. We introduce how this diagram can be used in a forward approach to make morphologic predictions, of (a) delta shoreline protrusion, (b) downstream channel widening, and (c) the number of distributary channels. We also introduce a new inverse approach that allows for estimating environmental conditions and sediment fluxes from morphological observations. Then, finally, for 31 deltas, we quantify the accuracy of the morphologic predictions.

## 2. Background

### 2.1. Delta Morphology as a Product of Its Environment

Deltas arise within the river source-to-sink sediment path (Bentley et al., 2016; Liu et al., 2009) when rivers debouche into a basin and their capacity for sediment transport is reduced (Gilbert, 1885). The resulting deposition forms topsets, foresets, and bottomsets, with morphologies shaped by a combination of terrestrial and marine processes (Patrino & Helland-Hansen, 2018; Wang et al., 2011). Terrestrial processes include rivers that mold mouth bars, create crevasse splays, and avulse channels, and whose morphologic effects are evident in the resulting distributary channel geometry and networks (Coffey & Shaw, 2017; Shaw et al., 2013), further affected by vegetation, waves, and tides (Anthony, 2015; Brückner et al., 2019; Passalacqua et al., 2013).

The sediment fraction that does not deposit at delta foresets and topsets continues its transit to the basin's bottom with an analogous set of dynamics controlling submarine deposits (e.g., Jobe et al., 2015; Naranjo-Vesga et al., 2020; Reading & Richards, 1994). These rich subaerial and submarine dynamics have long challenged predictions of delta morphology (Fagherazzi & Overeem, 2007; Gao et al., 2011; Olliver et al., 2020).

### 2.2. Where We Came From: Characterizing Delta Morphology

The seminal work that conceptualizes delta morphology as the result of the relative influence of terrestrial and marine processes includes Galloway's (1975). This contribution proposes a ternary diagram of delta morphology that represents the relative effect of the river, tides, and waves. River-dominated deltas attain a “bird-foot” morphology because the dominance of fluvial over marine fluxes enables mouth bar formation and maintenance of multiple distributary channels (Coleman & Wright, 1975; Edmonds & Slingerland, 2007; Ke et al., 2019). Conversely, waves tend to redistribute sediments near river mouths by alongshore and cross-shore fluxes (Komar, 1973). This process flattens shorelines and can seal river mouths (Jerolmack & Swenson, 2007; Nienhuis et al., 2015). As the third primary process, tides create in- and out-flow of water and sediments in river mouths, leading to estuarine morphologies (Dalrymple et al., 1992; Goodbred & Saito, 2012; Valle-Levinson, 2010) and channel loops (Konkol et al., 2022).

Inherent to Galloway's diagram and other works (Postma, 1995; Wright & Coleman, 1973) is the realization of a morphologic continuum of river deltas within river, tide, and wave-dominated end members. These end members include the traditional “bird-foot” deltas as river-dominated (e.g., Mississippi), funnel-shaped alluvial estuaries as tide-dominated (e.g., Fly), and river mouths with straight shorelines as wave-dominated (e.g., Eel and other small deltas). However, end members have traditionally not been well-defined, leading to extensions of the ternary diagram toward strandplains, tidal flats, and estuaries (Boyd et al., 1992; Nienhuis et al., 2020), which in turn produces debates on a quantitative definition of a delta that remains unresolved (Nienhuis et al., 2023; Syvitski et al., 2022; Zăinescu et al., 2023).

Other challenges from Galloway's diagram relate to quantifying the river, waves, and tide processes and their effect on delta morphology. Quantitative expressions assumed relevant for delta morphodynamics usually represent each process independently. For example, waves' potential to redistribute sediments alongshore was represented by wave power (Wright & Coleman, 1971, 1972), but comparison with similar river- and tidal power values proved difficult, and scaling issues arise when comparing relatively small and relatively big deltas (Syvitski & Saito, 2007). The resulting delta morphology was described as estuarine, lobate, or cusate, but was not quantified in morphometrics.

Delta morphology has also been analyzed outside the ternary diagram framework. Empirical approaches typically apply statistical models to values of environmental forcings and morphometrics, for example, obtaining delta area from river sediment supply or obtaining the number of distributary channels from fluvial discharge and wave power (J. D. Restrepo & López, 2008; Syvitski & Saito, 2007). These approaches are beneficial for upscaling, that

is, determining global delta area and investigating outliers, but gains in process understanding are limited. These studies argue that the (qualitative) ternary diagram approach is inappropriate because it cannot accommodate deltas with contrasting spatial scales. These works also acknowledge the gap in addressing delta morphology predictions with theoretical approaches. We aim to shrink these gaps by considering delta morphology from a physics-based parameter space within a quantitative Galloway ternary diagram.

### 2.3. Where We Are Now: Predicting Delta Morphology

Recent studies explored the quantification of Galloway's ternary relation as an integral predictive framework based on a physical coupling between delta morphology and the river, tides, and waves (Baumgardner, 2016; Konkol et al., 2022; Overeem et al., 2022; Seybold et al., 2007; Woodroffe et al., 2006 and others). In this vein, Nienhuis et al. (2020) extended Galloway's triangle as a quantitative framework of how much fluvial, wave, and tidal fluxes influence delta morphology.

A quantitative characterization of Galloway's ternary diagram consists of three steps. First, it requires a definition of the morphological characteristics that define each of the ternary axes. Wave-to-river dominance is expressed through cusped shorelines with a plan-view shoreline protrusion that increases with decreasing wave influence. Wave-dominated deltas have a high likelihood of littoral spit formation and alongshore sediment bypassing (Alcántara-Carrió et al., 2019; Ashton & Giosan, 2011; Broaddus et al., 2022; Dan et al., 2011). Once deltas pass a threshold and become river-dominated, they branch and develop multiple distributary channels (Olariu & Bhattacharya, 2006; Syvitski & Saito, 2007). River-to-tide dominance is expressed as increasing downstream channel widening as nearshore morphology must accommodate oscillatory volumes of water moved by tides (Goodbred & Saito, 2012; Rossi et al., 2016). Thresholds are less clear between river- and tide-dominated deltas. Arguably, one process threshold could be that deltas become tide-dominated when tides are large enough to reverse the river flow at the river mouth (Langbein, 1963; Z. Xu & Plink-Björklund, 2023). Lastly, fluvial dominance expresses itself by the absence of wave or tidal influence, exhibiting crenulated (as opposed to straight) shorelines, several distributary channels, and limited downstream channel widening.

The second step is understanding how wave, tidal, and river processes create delta morphology. The new theory enabled quantitative relations in terms of the mass flux of sediment. Theories link downstream channel widening and shoreline orientation as a function of fluvial sediment loads toward river mouths and wave-driven and tide-driven sediment loads away from river mouths (Nienhuis et al., 2015, 2018). Building on this ternary approach, other studies have added further empirical morphological characterizations of deltas (Broaddus et al., 2022; Vulis et al., 2023).

In the third step, the sediment mass fluxes at the river mouth are predicted using formulations of only upstream fluvial characteristics and offshore tidal and wave characteristics. Although river, wave, and tidal sediment fluxes can be measured directly in the field, such measurements are sparse. An a priori prediction based on wave, tidal, and river boundary conditions enables the use of widely (globally) available data. These boundary conditions can then be reformulated to represent the capacity to move sediments near river mouths and the resulting delta morphology.

The quantitative ternary diagram supports a continuum of coastal morphologies of wave, tide, and river sediment flux ratios. There is no inherent lower limit to the fluvial sediment flux, even though the term river delta becomes increasingly incorrect for vanishingly small river sediment deposits. This limitation was recognized before by Dalrymple et al. (1992) and Boyd et al. (1992), attempting to quantify coastal alluvial morphologies. Therefore, the quantified ternary diagram can also be considered to characterize a collection of coastal alluvial morphologies near river mouths, including deltas, strandplains, and estuaries, given that no quantitative criteria exist yet to separate these morphologies.

Another implication of the quantified ternary approach is that it is based on a sediment flux balance and includes the first-order effects of sediment characteristics on delta morphology (Burpee et al., 2015; Edmonds & Slingerland, 2010). For example, sediment size differs between the wave, river, and tidal sediment fluxes, making the number of distributary channels in river-dominated deltas dependent on the proportion of fine sediment (Caldwell & Edmonds, 2014). Earlier energetics-based approaches did not include grain size and required added dimensions in the ternary space (Orton & Reading, 1993).

A downside of the quantified ternary approach is that it is based on the balance between fluvial sediment fluxes at the river mouth—data that may be difficult to acquire. Channel bifurcations unequally partition the fluvial sediment flux at individual river mouths compared to the delta apex (for which river data is most often available) (Federici & Paola, 2003; Kleinhans et al., 2013). The tidal sediment flux depends on the tidal prism, which decreases as channels split and narrow but varies nonlinearly with the number of distributary channels (Frings & Kleinhans, 2008; Sassi et al., 2011). The wave sediment flux acts on each river's mouth. Therefore, deltas can bifurcate themselves into tide- or wave-dominance and show multiple dominances in different delta lobes (Giosan et al., 2006). Although interesting, predicting the morphology at individual lobes requires information about how the sediment flux splits at distributary junctions. To avoid this complication, Nienhuis et al. (2020) predicted one morphological dominance for each delta based on the sediment flux at the apex. This approach provides a first-order prediction but does not represent the morphodynamics entirely.

In the case of fluvial fluxes, sediment trapping on delta plains upstream of river outlets and bypassing offshore of river mouths may also reduce the fluvial sediment available for redistribution at the river mouth. Estimates suggest that ~30% of the fluvial sediment load may be trapped on delta plains (Paola et al., 2011). Still, because of limited data, its effect on delta morphology has not been widely explored.

#### 2.4. The Next Step: Quantifying Prediction Uncertainty

The quantified ternary approach presents a theoretical advance and a reasonable step toward a global predictive model of delta morphology (Hoitink et al., 2020). But how accurate is it? A qualitative comparison with observations, that is, whether observed wave-dominated deltas (as deduced by the level of shoreline “flatness” and the lack of distributary formation) were predicted to be wave-dominated, shows that 85% of the deltas (265 out of 312) are classified correctly (Nienhuis et al., 2020). But, whether the delta morphological characteristics of channel widening, shoreline protrusion, and the number of distributary channels are predicted accurately within the ternary diagram remains an open question.

Our key advance is a set of methods to align predictions and observations of deltaic forcing conditions and delta morphology within Galloway's ternary diagram. We predict morphology using the balance of sediment fluxes from boundary conditions and show a new inverse approach where we infer boundary conditions and the sediment flux balance from delta morphological observations. With this novel approach, we can compare predictions with observations and provide a measure of prediction accuracy for sediment fluxes and morphological metrics. We do this for 31 deltas, a selection that represents a range of morphologies, including some of the largest fluvial catchments, representative end-member morphologies, and deltas from a relatively under-studied region (Best, 2019; Galloway, 1975; Nienhuis et al., 2020; J. D. Restrepo & López, 2008).

### 3. Methods

In this methods section, we will first describe the ternary framework for delta morphology (Section 3.1) and then the methodology for morphologic predictions from Nienhuis et al. (2020) (Section 3.2, green in Figure 1). We will add our new contribution, an inverse approach that ties observations into the same framework (Section 3.3, orange in Figure 1), to finally compare predictions with observations and determine the accuracy (Section 3.4, gray in Figure 1).

#### 3.1. Sediment Flux Balance at Deltas

At the heart of the quantitative Galloway's ternary diagram sits a sediment flux balance (Figure 2). The sediment flux balance compares the riverine sediment discharge ( $Q_{river}$ ,  $\text{kg s}^{-1}$ ), with the maximum potential sediment transport by waves alongshore away from the river mouth ( $Q_{wave}$ ,  $\text{kg s}^{-1}$ ), and the amplitude of tidal sediment discharge at the river mouth across a tidal cycle ( $Q_{tide}$ ,  $\text{kg s}^{-1}$ ). We provide the derivations in Sections 3.2 and 3.3.

The three sediment fluxes can be used to derive a tripartite relative sediment flux  $r_x$  (where  $x$  corresponds to *river*, *wave*, or *tide*), as



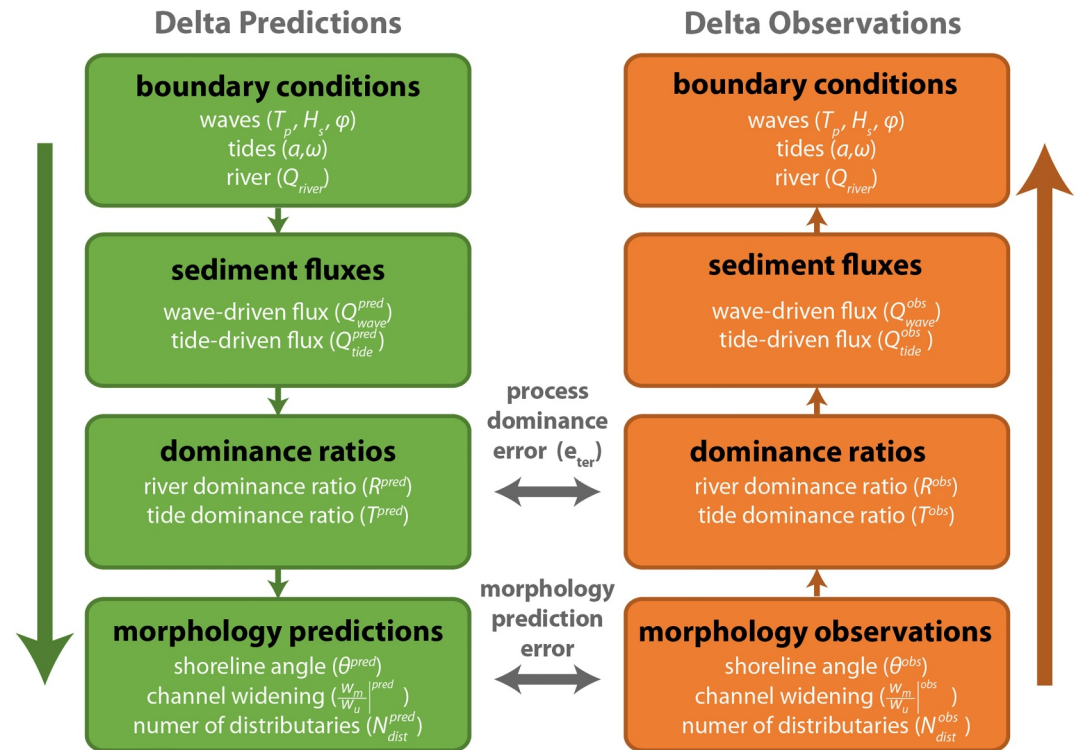


**Figure 1.** General methods workflow: Generating delta morphology predictions through sediment fluxes from boundary conditions (green) and using morphology observations to assess the predictions and allow delta sediment fluxes (orange) estimation. Boundary conditions also include general morphometrics, that is, reference shoreline angle, delta slope, and fluvial channel width. Errors can be determined for both process dominance and morphology. Note that sediment fluxes can also be observed directly (i.e., without inferring them from the morphology) if data are available.

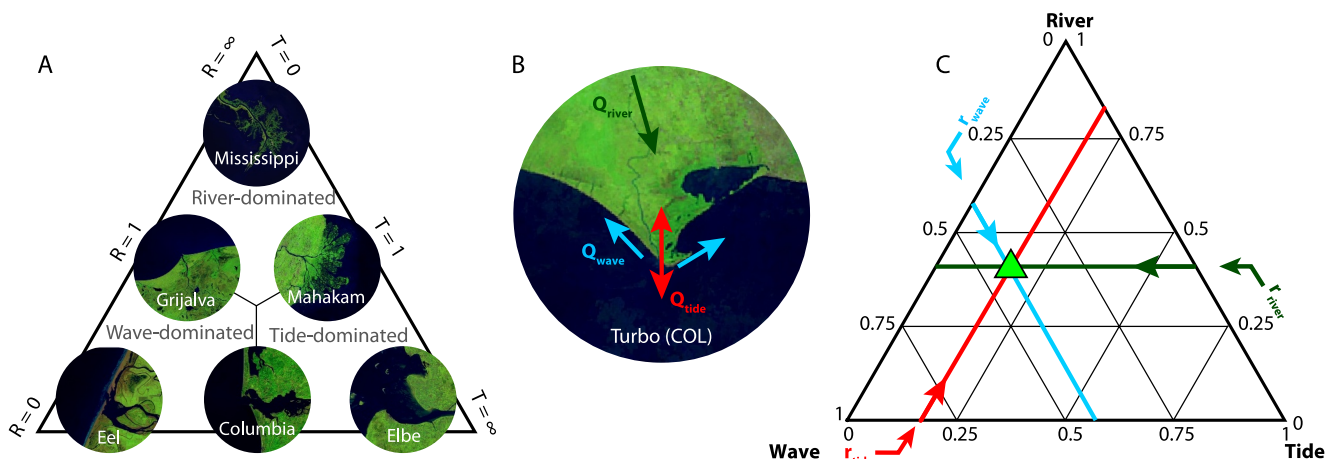


**Figure 2.** The Galloway ternary diagram, represented as (a), the river- and tide-dominance ratios ( $R$  and  $T$ ) and the resulting process dominance, modified from Nienhuis et al. (2020, their Figure 1a). (b) Schematic of the sediment flux balance by river, waves, and tides for Turbo River delta, Colombia. (c) The Galloway ternary diagram with the location of a hypothetical delta, with relative fluxes,  $r_{river} = 0.4$  (dark green),  $r_{wave} = 0.4$  (blue), and  $r_{tide} = 0.2$  (red). The intersection (light green triangle) shows the location of the hypothetical delta within the quantitative ternary diagram. Red, blue, and green arrows indicate the direction for drawing lines of constant values of the corresponding  $r_x$  values. Imagery by Aquamonitor (Donchyts et al., 2016, <https://aqua-monitor.appspot.com/>).

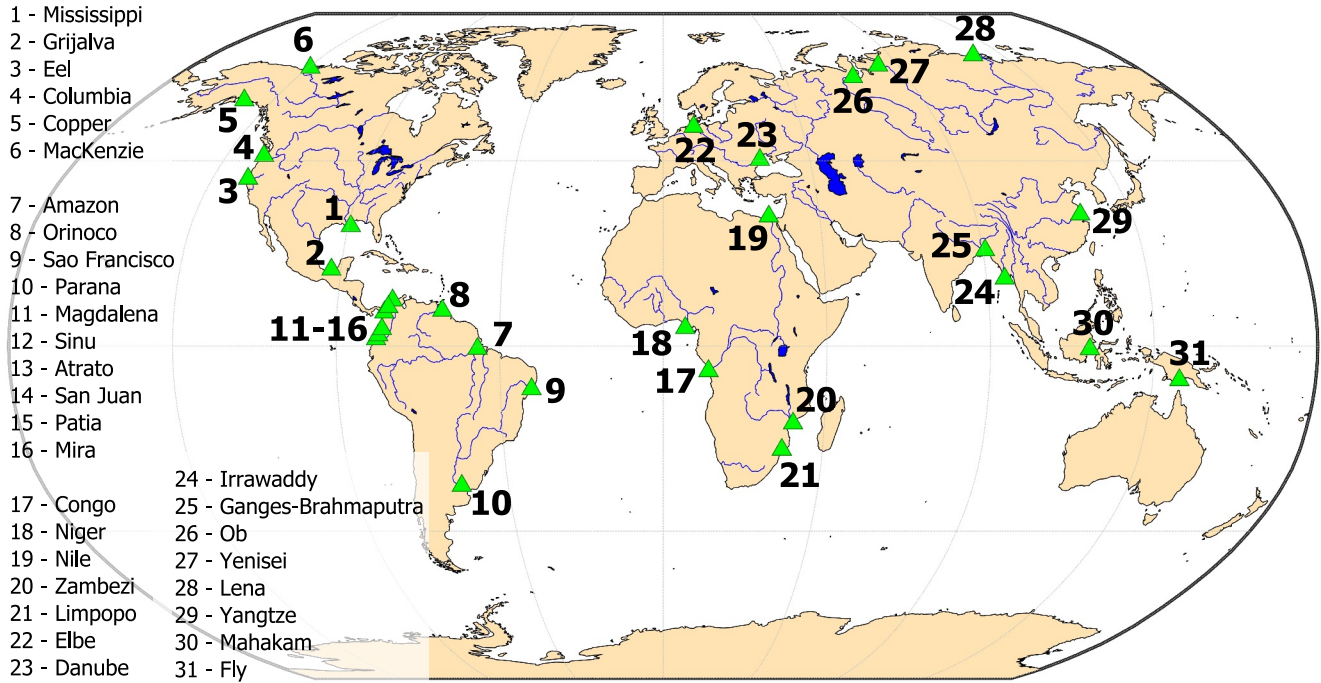


**Figure 3.** Location of 31 deltas assessed in this study in North America, South America, Africa, Europe, Asia, and Oceania. Delta numbers 11–16 correspond to the major Northern Andes deltas (see Figure 4 for their location). Map from the M\_Map routine (Pawlowicz, 2020).

$$r_{river} = \frac{Q_{river}}{Q_{river} + Q_{wave} + Q_{tide}}, \quad (1)$$

$$r_{wave} = \frac{Q_{wave}}{Q_{river} + Q_{wave} + Q_{tide}},$$

and

$$r_{tide} = \frac{Q_{tide}}{Q_{river} + Q_{wave} + Q_{tide}},$$

such that  $r_{tide} + r_{wave} + r_{river} = 1$ , with the sediment fluxes defined below. Each ratio represents the fraction of the total sediment flux that each process contributes. If all processes move the same quantity of sediments, then  $r_{river} = r_{wave} = r_{tide} = 0.3$ . For example, for a delta with  $r_{river} = 0.4$ ,  $r_{wave} = 0.4$ , and  $r_{tide} = 0.2$  (Figure 2b), we locate values along its axis and draw a line following the arrows. Once we obtain the relative sediment fluxes, we know the process dominance by plotting these relative fluxes within a ternary diagram. Each relative flux corresponds to an axis within the chart, and dominances reflect delta morphology according to each axis (Figure 2c).

The three sediment fluxes can also be cast as two 1-dimensional ratios: the fluvial ( $R$ ) and tidal ( $T$ ) dominance ratios (Nienhuis et al., 2015, 2018). These 1-dimensional factors have a straightforward relation to their 2-dimensional ternary cousins as

$$R = \frac{Q_{river}}{Q_{wave}} = \frac{r_{river}}{r_{wave}}, \quad (2)$$

and

$$T = \frac{Q_{tide}}{Q_{river}} = \frac{r_{tide}}{r_{river}}. \quad (3)$$

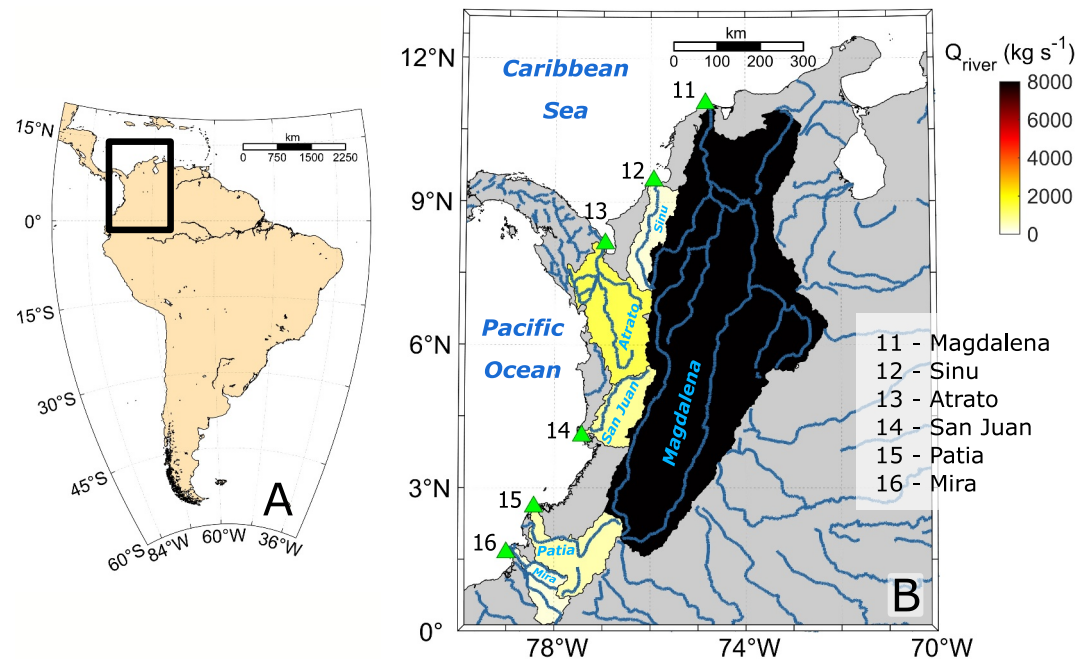


**Figure 4.** Location of Northern Andes deltas in this study (11–16) in the Northwestern South American coastal zone marked by green triangles in (a) South America and (b) showing main streams, catchment areas, and pristine fluvial sediment flux ( $Q_{river}$ ). Maps from the M\_Map routine (Pawlowicz, 2020).

The primary use of the dominance ratios is that they can be linked to delta morphology. The  $R$  factor represents river-to-wave dominance, with high wave dominance (low  $R$ ) resulting in a straight coastline (little delta protrusion). High fluvial dominance leads to more significant delta protrusion, with multiple distributaries predicted for  $R > 1$ .

Similarly, the  $T$  factor represents tide dominance by comparing the amplitude of tidal sediment discharge at the river mouth ( $Q_{tide}$ ,  $\text{kg s}^{-1}$ ) to the fluvial sediment discharge ( $Q_{river}$ ). Tidal dominance ( $T > 1$ ) results in flow reversal at the river mouth and downstream widening of the river channel (an estuarine “funnel” morphology), whereas  $T < 1$  results in a small downstream tide-driven change in river mouth width (Nienhuis et al., 2018).

### 3.2. Delta Predictions

We used the sediment flux balance to predict delta morphology for 31 deltas, following the flowchart (Figure 1) and starting with delta boundary conditions.

#### 3.2.1. Delta Boundary Conditions

We retrieve the mean fluvial sediment flux toward the delta at the delta apex ( $Q_{river}$ ,  $\text{kg s}^{-1}$ ) from two sources. We use two data compilations for 18, mostly large deltas (Overeem et al., 2022; Syvitski & Saito, 2007) that report the combined bed- and suspended transport load. For the remaining 13 deltas, we estimate  $Q_{river}$  as the long-term (>30 years) average suspended sediment load from the empirical WBMSed 2.0 model (Cohen et al., 2014) that uses basin temperature, lithology, and other factors to estimate sediment loads.

For waves, we retrieve a 30-year record of significant wave height ( $H_s$ , m), mean wave period ( $T$ , s), and mean wave direction ( $\phi_0$ , degrees true or °) from the WAVEWATCH III reanalysis (Chawla et al., 2013) for a computational node closest to each delta. Note that the use of WAVEWATCH III does not imply that our methods rely on global models of wave statistics; our method can also be applied using wave data that can be measured with moored instrumentation, if available. For tides, we use the TPXO tidal reanalysis product (Egbert & Erofeeva, 2002; Egbert et al., 1994) to obtain the tidal amplitude and angular frequency for the main tidal constituents near each delta. We use the largest tidal constituent to represent the multiyear average amplitude. Other boundary

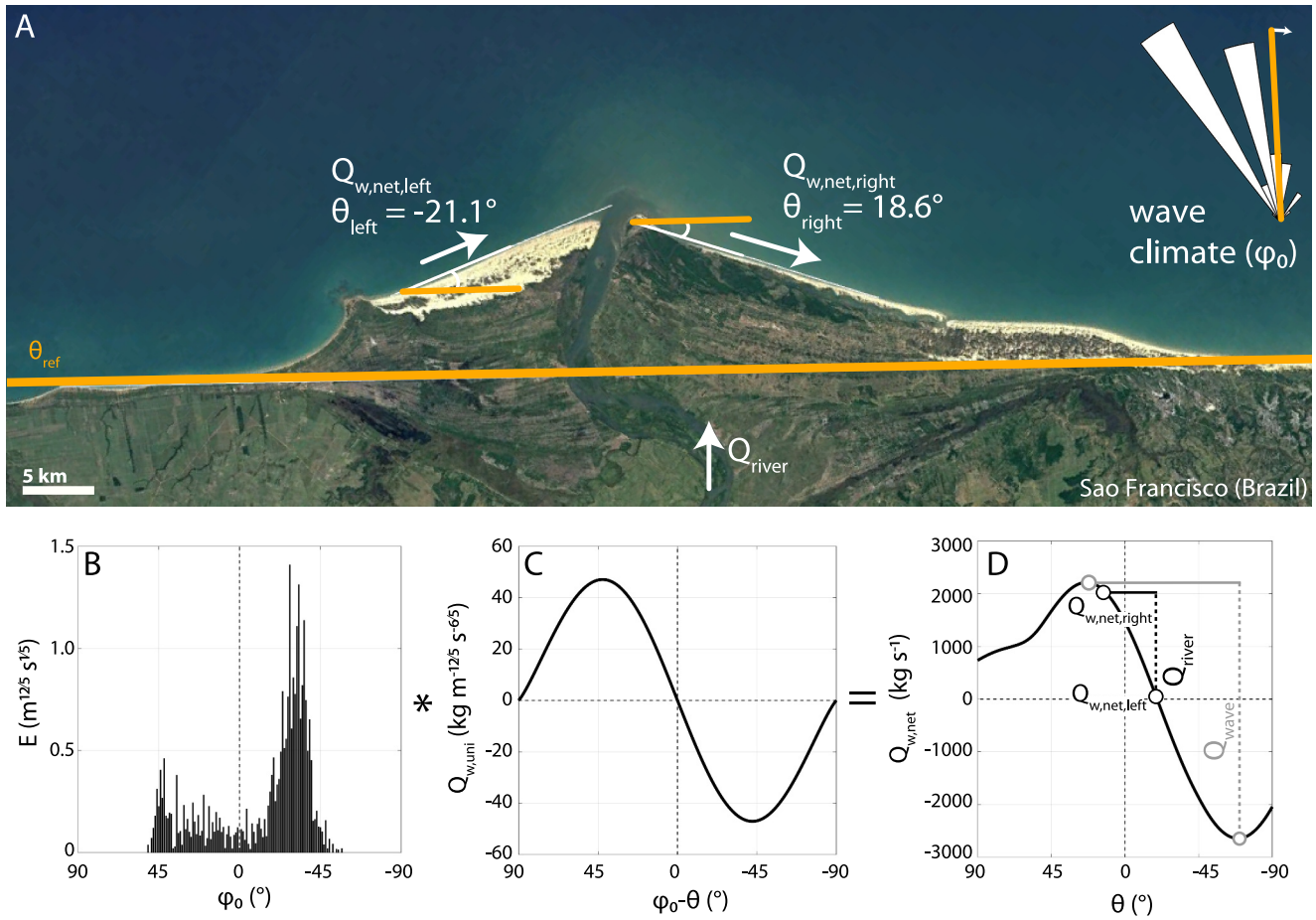


**Figure 5.** An example of computing  $Q_{w,net}$  and  $Q_{wave}$  for the Sao Francisco River delta on the Brazilian coast. (a) The Sao Francisco delta showing morphology and wave climate distribution. We obtained flank angles from Google Earth® imagery ( $\phi_0$ ,  $\theta_{left}$ , and  $\theta_{right}$  in  $^\circ$  with respect to the reference shoreline in orange). (b) Wave energy distribution as a function of wave approach angle from WAVEWATCH simulations (Chawla et al., 2013). (c) Unitary wave alongshore transport as a function of wave-to-shoreline approach angle. (d) Net alongshore sediment transport as a function of shoreline angle. Gray circles show the net transport expected at the left and right flanks ( $Q_{w,net,l}$  and  $Q_{w,net,r}$ ). The gray bar shows the maximum potential sediment flux away from the river mouth ( $Q_{wave}$ ) along the left and right flanks. The black bar shows the actual sediment flux difference between the left and right flanks, which, if sediment is conserved nearshore, is equal to  $Q_{river}$ . Symbols between panels B through D (asterisk and equal) represent the convolution operation to quantify  $Q_{w,net}$  (see text).

conditions needed to compute the tidal sediment flux are the upstream channel depth, which we obtain from measuring channel width and hydraulic geometry relations, and the delta slope, which we obtain from Google Earth's imagery and SRTM elevation data.

### 3.2.2. Predicting $Q_{wave}^{pred}$

From the boundary conditions, we first predict  $Q_{wave}^{pred}$ , representing the maximum potential alongshore sediment flux by waves away from the river mouth along any shoreline angle (in units of  $kg s^{-1}$ ). This quantity is the sum of the maximum potential transport from the river mouth to the right and left (Nienhuis et al., 2015, their Supp. Info.) (Figure 5).

The  $Q_{wave}^{pred}$  can be derived from wave climate analysis alone, and it does not require delta morphology observation beyond a reference shoreline orientation of the non-deltaic coast. It is given by

$$Q_{wave}^{pred} = \max[Q_{w,net}(\theta)]_{-\pi \leq \theta \leq 0} - \min[Q_{w,net}(\theta)]_{0 \leq \theta \leq \pi} \quad (4)$$



where the observed net alongshore sediment transport,  $Q_{w,net}$ , is a function of the shoreline angle  $\theta$  and is obtained by convolving the mean wave-energy angle distribution,  $E(\phi_0)$ , and the alongshore sediment transport for a unitary wave from a single direction,  $Q_{w,uni}(\phi_0 - \theta)$ ,

$$Q_{w,net}(\theta) = E(\phi_0) * Q_{w,uni}(\phi_0 - \theta), \quad (5)$$

where the operator  $[\ast]$  indicates convolution,  $\theta \in (-\frac{\pi}{2}, \frac{\pi}{2})$  is the angle of potential delta shorelines to the reference shoreline orientation,  $\theta_{shore}$  (so  $0^\circ$  is a shoreline aligned with the reference shoreline, and  $-90^\circ$  and  $90^\circ$  are shorelines perpendicular to the reference shoreline), and  $\phi_0$  is the angle of wave approach (in deep water) to the reference shoreline (Figure 5). The difference  $\phi_0 - \theta$  refers to the angle of the wave approach relative to the delta flank shoreline.

We calculate the wave energy  $E(\phi_0)$ , in  $\text{m}^{12/5} \text{s}^{1/5}$ , as:

$$E(\phi_0) = \frac{\sum_{\phi_0} [H_s^{12/5}(\phi_0) T^{1/5}(\phi_0)]}{n}, \quad (6)$$

where  $H_s$  (m) is the significant wave height,  $T$  (s) is the wave period, and  $n$  is the number of observations.

The alongshore sediment transport distribution,  $Q_{w,uni}$  (in  $\text{kg} \cdot \text{m}^{-12/5} \text{s}^{-6/5}$ ), is based on the alongshore sediment transport function (Ashton & Murray, 2006 their Equation 5) for unitary offshore (or un-refracted) wave energy, that is, for  $H_s = 1$  m and  $T = 1$  s, as

$$Q_{w,uni} = K_{wave} \rho_b \cos^{6/5}(\phi_0 - \theta) \sin(\phi_0 - \theta), \quad (7)$$

where  $K_{wave} \approx 0.06 \text{ m}^{3/5} \text{s}^{-6/5}$  is an empirical constant (Nienhuis et al., 2015) and  $\rho_b$  is the bulk density of sediments ( $= 1,600 \text{ kg m}^{-3}$ ).

In this study, we use Equations 4–7 to estimate ( $Q_{wave}^{pred}$ ). But, if any reader is interested in estimating  $Q_{wave}^{pred}$  but does not know the distribution of wave approach angles, there is a simplified method. Suppose one assumes that the wave approach is perpendicular to the delta shoreline. In that case, there is no wave sheltering, and the transport maximum (to the right) and the minimum (to the left) have the same absolute magnitude. Then, the maximum potential transport away from the river mouth ( $Q_{wave}^{pred}$ , Equation 4) simplifies to

$$Q_{wave}^{pred} \approx 2 \cdot K_{wave} \cdot \rho_b \cdot H_s^{12/5} \cdot T^{1/5} \cdot 0.47. \quad (8)$$

### 3.2.3. Predicting $Q_{tide}^{pred}$

We calculate  $Q_{tide}^{pred}$ , defined as the tide-driven sediment flux amplitude ( $\text{kg s}^{-1}$ ) at the river mouth for the dominant (i.e., with the largest amplitude) tidal constituent as

$$Q_{tide}^{pred} = \frac{1}{2} \omega k_{tide} a^2 L^2 \beta f c, \quad (9)$$

where  $a$  is the offshore tidal amplitude (m),  $\omega$  is the tidal angular frequency in radians per second,  $k_{tide} = \frac{\omega}{\sqrt{\theta D_{50} R C_z \pi}} \text{ (m}^{-1}\text{)}$  is a sediment transport coefficient ( $\approx 1.1 \times 10^{-4} \text{ m}^{-1}$  for semi-diurnal tides, and  $5.7 \times 10^{-5} \text{ m}^{-1}$  for diurnal tides),  $R$  is the submerged specific gravity ( $\approx 1.65$ ),  $\theta$  is the Shields number under active conditions ( $\approx 0.2$ ),  $D_{50}$  is the median grain size (0.1 mm here), and  $C_z$  is the Chezy roughness ( $55 \text{ m}^{1/2} \text{s}^{-1}$  here). The value  $\beta = \frac{w_u}{d_u}$  is the fluvial channel aspect ratio, where  $w_u$  is the fluvial channel width and  $d_u = 0.6 \cdot Q_{w,river}^{1/3}$  (Mikhailov, 1970, Eq. 21) is the channel depth. In addition,  $f = 1 + \frac{2S}{ka}$  (with  $S$  as the mean delta channel slope),  $L$  is a characteristic estuarine length (or estuary length, defined as  $d_u/S$ ),  $c$  is the sediment concentration ( $\text{kg m}^{-3}$ ), assumed equal to the river sediment concentration, derived from the mean annual



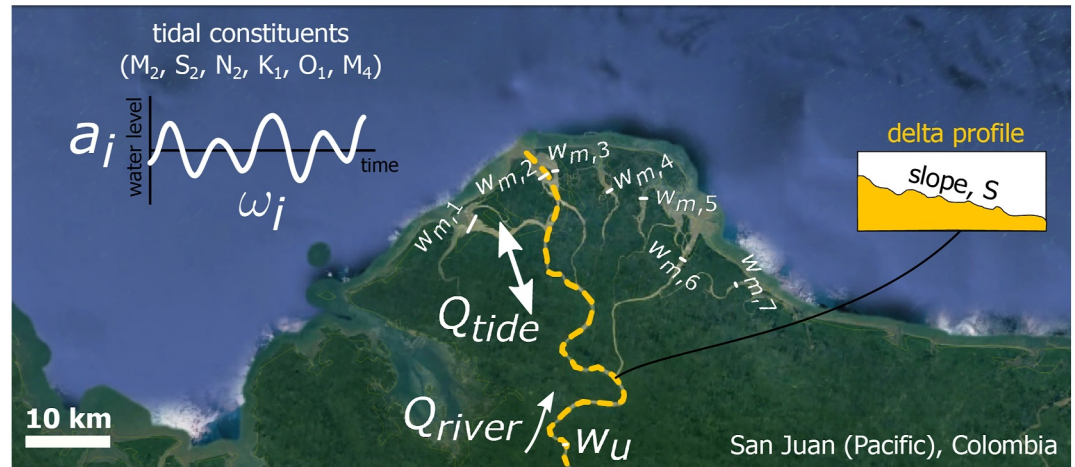


**Figure 6.** Metrics involved in predicting and observing the sediment flux by tides,  $Q_{tide}$ , from delta morphology, as given for the San Juan River delta (Colombia). In this case, there are seven distributary mouths, with a channel width for each mouth ( $w_{m,1}$ , etc.), measured from the Google Earth® imagery. We calculated the delta slope along the transect in yellow from the average elevation change and distance. We represent tidal properties by amplitudes and frequencies of tidal constituents (Egbert & Erofeeva, 2002). We use  $Q_{river}$  to estimate the fluvial channel depth (see text for explanation).

sediment flux  $Q_{river}$  ( $\text{kg s}^{-1}$ ), and the mean annual water discharge (in  $\text{m}^3/\text{s}$ ) (Figure 6). Derivation of Equation 9 can be found in Nienhuis et al. (2018).

### 3.2.4. Predicting Delta Morphology

From the three sediment fluxes ( $Q_{river}$ ,  $Q_{tide}$ ,  $Q_{wave}$ ) we obtain two dominance ratios ( $R$ ,  $T$ ) that we use to predict three morphological characteristics: the delta shoreline angle ( $\theta^{pred}$ ), the number of distributary channels ( $N_{dist}^{pred}$ ), and the river mouth channel widening ( $\left(\frac{w_m}{w_u}\right)^{pred}$ ). The first two ( $\theta^{pred}$  and  $N_{dist}^{pred}$ ) depend on the ratio  $R$  (left leg of the triangle), and  $\left(\frac{w_m}{w_u}\right)^{pred}$  depends on  $T$  (right leg of the triangle, Figure 7).

Note that the shoreline angles and the number of distributary channels are mutually exclusive predictions. We either predict deltas to have cusped shorelines with a defined  $\theta^{pred}$  and one distributary channel ( $N_{dist}^{pred} = 1$ ), or we predict multiple distributary channels ( $N_{dist}^{pred} > 1$ ) and an undefined  $\theta^{pred}$ . This choice relates to an “entire delta” focus instead of individual distributaries for which we could quantify different degrees of wave, river, and tidal influence, but which then requires knowledge of sediment flux distribution within the distributary network.

Note also that deltas, of course, have many more morphological characteristics that we do not predict (e.g., delta elevation, delta area, and channel network structure). We focus on the delta shoreline angle ( $\theta^{pred}$ ), the number of distributary channels ( $N_{dist}^{pred}$ ), and the river mouth channel widening ( $\left(\frac{w_m}{w_u}\right)^{pred}$ ) because for these three we have theoretical expectations that we can derive from delta boundary conditions.

### 3.2.5. Predicting Delta Shoreline Angle

The first morphologic prediction is of the delta shoreline angle ( $\theta^{pred}$ ). In the case of  $R < 1$ , all delivered river sediment is transported alongshore along both delta flanks and, therefore assumed, equal to the difference between the wave-driven alongshore fluxes ( $Q_{w,net}$ , Figure 5d). Because  $Q_{w,net}$  is a function of the shoreline angle, we can rewrite it so that we predict the shoreline angle based on a known  $Q_{w,net}$ . If the wave approach is symmetric, then each flank conveys half the fluvial sediment flux, and  $\theta^{pred}$  (in  $^\circ$ ) is

$$\theta^{pred} = Q_{w,net}^{-1} \left( \pm \frac{1}{2} Q_{river} \right), \quad R < 1, \quad (10)$$

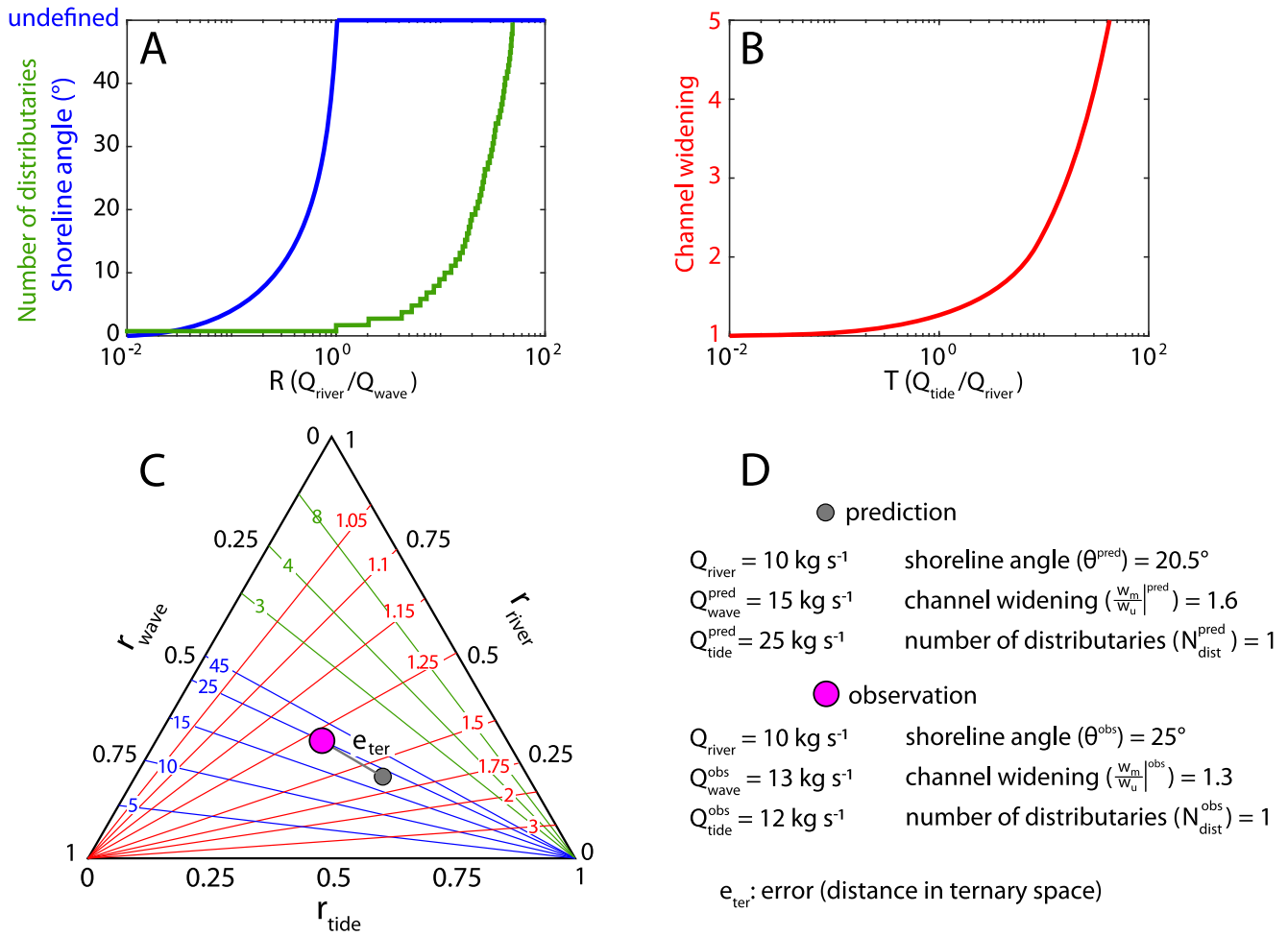


**Figure 7.** Relations between the delta sediment flux balance and its morphology within the quantitative Galloway ternary diagram. (a) Variation in shoreline angle and number of distributary mouths as a function of the fluvial dominance ratio  $R = \frac{r_{river}}{r_{wave}}$ , for an example of wave climate and following Equation 10. Note that the specific relation will deviate for different wave climates. (b) Variation in downstream channel widening with the tidal dominance ratio  $T = \frac{r_{tide}}{r_{river}}$ , for a single dominant constituent and a delta slope. Note that the relation will deviate with different tidal properties and slopes. (c) Morphological predictions cast into the quantitative ternary diagram, with contour lines and numbers indicating (in blue) the shoreline angle, (in green) the number of distributary channels, and (in red) the channel widening. The exact numbers will deviate depending on second-order characteristics. (d) Example predictions (in gray) and observations (in magenta), with  $Q_{river} = 10 \text{ kg s}^{-1}$ ,  $Q_{wave} = 15 \text{ kg s}^{-1}$ , and  $Q_{tide} = 25 \text{ kg s}^{-1}$ , for which we predict a  $20.5^\circ$  protrusion angle, channel widening of 1.6 (mouth is 60% wider than the upstream channel), and a single distributary mouth ( $R < 1$ ). The magenta circle shows the hypothetical delta morphology observations (widening of 1.3, shoreline angle of  $25^\circ$ , and 1 distributary channel). Error ( $e_{ter}$ ) corresponds to the distance between predictions and observations within the ternary diagram.

which can be obtained graphically (Figure 5d): starting at  $\theta = 0$ , with a certain  $Q_{w,net}(\theta = 0)$ , following the function for  $Q_{w,net}$  in the positive and negative directions. The  $\theta^{pred}$  are then the shoreline angles (positive and negative) where the difference in the resulting flux equals the fluvial sediment flux ( $Q_{river}$ ). In other words:  $Q_{w,net}(\theta_{right}^{pred}) - Q_{w,net}(\theta_{left}^{pred}) = Q_{river}$ . Although it is possible to make predictions for each flank (Nienhuis, Ashton, & Giosan, 2016), in this study we report the average angle.

Equation 10 can be further simplified if the wave approach has a low directional spread. In this case,  $Q_{w,net}$  approaches  $Q_{w,uni}$  (Equation 7), and the simplest solution is obtained from writing

$$R = \frac{Q_{river}}{Q_{wave}} = \frac{Q_{w,uni}}{\max(Q_{w,uni})} = \frac{\cos^{\frac{5}{6}} \theta \sin \theta}{\max(\cos^{\frac{5}{6}} \theta \sin \theta)} \approx \frac{\frac{1}{2} \sin(2\theta)}{\frac{1}{2}}. \text{ From this rationale, it follows that}$$

$$\theta^{pred} \approx \frac{1}{2} \arcsin\left(\frac{Q_{river}}{Q_{wave}}\right) \quad R < 1. \quad (11)$$

In the case of  $R > 1$ , Equations 10 and 11 are undefined. There are no shoreline angles possible that could convey the fluvial sediment flux, and we predict a river-dominated delta with undefined  $\theta^{pred}$  (Figure 7).

### 3.2.6. Predicting Distributaries

The second morphologic prediction is for the number of distributary channels,  $N_{dist}^{pred}$ . In the original framework (Nienhuis et al., 2015, 2018), the fluvial dominance ratio  $R$  did not provide morphological predictions for river-dominated deltas ( $R > 1$ ). Here, we add a prediction for the number of distributary mouths, following other contributions (Broaddus et al., 2022), to quantify the degree of river dominance.

We propose the following rationale: if  $R > 1$  (river dominated), waves cannot move all the fluvial sediment away from the river mouth, then mouth bars will form that will split the channel and create multiple river mouths (e.g., Edmonds & Slingerland, 2007). The fluvial sediment flux is then distributed between the mouths, whereas the maximum (potential) alongshore sediment flux ( $Q_{wave}$ ) remains the same for each river mouth. Therefore, we predict that the process of mouth bar and distributary channel formation continues until the river sediment load per distributary ( $Q_{river}/N_{dist}^{pred}$ ) falls below the potential alongshore flux ( $Q_{wave}$ ), that is,

$$N_{dist}^{pred} = \left\lceil \frac{Q_{river}}{Q_{wave}} \right\rceil, \quad (12)$$

where the operator  $\lceil \cdot \rceil$  represents rounding up to the next integer. In other words, wave-dominated deltas have one river mouth because the ratio is less than 1. For river-dominated deltas, each river mouth provides enough sediment to balance alongshore sediment transport away from the river mouth. Equation 12 follows the same physical principles of other empirically derived equations (J. D. Restrepo & López, 2008 their Table 5; Syvitski & Saito, 2007 their Equation 4).

### 3.2.7. Predicting Downstream Widening

The third morphological prediction is for the downstream channel widening,  $w_m/w_u$ , as

$$\left. \frac{w_m}{w_u} \right|^{pred} = \frac{Q_{tide}}{Q_{river} U f} + 1, \quad (13)$$

where  $U = \frac{0.5\omega a}{S \cdot u_{river}}$  is the strength of the tidal flow of the largest tidal constituent relative to the fluvial flow ( $u_{river}$ ) with the quantities defined in Equation 9 (Nienhuis et al., 2018). Deltas that have a relatively large  $\frac{Q_{tide}}{Q_{river}}$  (e.g., alluvial estuaries like the Elbe) are predicted to have  $w_m \gg w_u$ , whereas deltas with negligible tidal influence (e.g., Grijalva) should have  $w_m \approx w_u$ . We include the relations between tidal dominance and morphology in Figure 7b for given values of  $U$  and  $f$ . Overall, channel widening will increase for more significant tidal fluxes relative to the fluvial fluxes.

## 3.3. Delta Observations

### 3.3.1. Retrieving Morphology Observations

We compare our predictions of delta morphology against observations using imagery from Google Earth Pro®. For 31 deltas, we retrieved the shoreline angles, the number of distributary channels, and the river mouth and upstream channel widths (see Paniagua-Arroyave & Nienhuis, 2024, for Supplemental Data).

Shoreline angle observations were retrieved by digitizing the angle of each delta flank ( $\theta_{left}^{obs}$  and  $\theta_{right}^{obs}$ ) relative to the reference shoreline ( $\theta_{ref}$ ), that is, by marking two points from left to right looking offshore. We then cast the difference angle into one of three quadrants depending on the flank (whether left or right), such that each quadrant represents a morphodynamic state: cusate, crenulated, or estuarine.

The cusate condition refers to the typical delta shape with straight delta flanks protruding seaward toward the river mouth. The crenulated condition occurred when we observed a river-dominated delta with several distributaries ( $N_{dist} > 1$ ) and without straight flanks. In this case, both  $\theta^{obs}$  angles are undefined. Although in some

cases  $\theta^{obs}$  angles can be defined for deltas for multiple distributaries (e.g., Nile, Sinu), it is difficult to incorporate it into our ternary framework because it would, under our assumptions, make a delta simultaneously river- and wave-dominated. A lobe-based analysis is a possible solution, but this is a departure from the rest of our analysis and therefore not undertaken here.

Estuarine conditions occurred when delta flanks protruded landward instead of seaward, such as the delta shape resembling the “funnel” shape (seaward increase in channel width) of single thread tide-dominated deltas (e.g., Elbe). Note that we could include a “spit” condition (the fourth quadrant) when the flanks form an “inverse funnel” shape such that channel width decreases seaward, as in a funnel-shaped distributary with nearshore spits narrowing its outlet. Such a condition likely arises when the channel is not fully alluviated and does not fit our ternary diagram. We excluded it.

In addition to the flank angles, we counted the number of distributary mouths ( $N_{dist}^{obs}$ ) and measured each river's mouth width by digitizing a straight line perpendicular to the delta distributary banks closest to the ocean. We obtained the channel-widening fraction  $\frac{w_m}{w_u}|^{obs}$  from the sum of distributary widths as  $w_m = (N_{dist}^{obs})^{-0.5} \sum_{n=1}^{N_{dist}^{obs}} w_{m,n}$  (Nienhuis et al., 2018) (Figure 6) and compared it to the upstream channel width,  $w_u$ , measured at the upstream limit of tidal influence.

### 3.3.2. Observed River Dominance

Using our morphologic observations, we can infer wave, river, and tidal sediment fluxes through the estimation of the river dominance ratio ( $R^{obs}$ ) and the tide-dominance ratio ( $T^{obs}$ ). Note that this inference relies on our morphologic observations and on data that were also used to predict sediment fluxes. Given that they are derived from morphologic observations, we refer to these sediment fluxes as “observations” in contrast to the sediment fluxes derived from boundary conditions (Figure 1). We discuss the implications of this choice in our Discussion (Section 5.1).

First, the observed river dominance ratio,  $R^{obs}$ , can be estimated by

$$R^{obs} = N_{dist}^{obs}, N_{dist}^{obs} > 1, \quad \text{or} \quad (14)$$

$$R^{obs} = \frac{Q_{w,net}^{obs}}{Q_{wave}^{pred}} = \frac{Q_{w,net}(\theta_{right}^{obs}) - Q_{w,net}(\theta_{left}^{obs})}{Q_{wave}^{pred}}, N_{dist}^{obs} = 1.$$

The first relation holds when none of the distributaries discharge more sediment than  $Q_{wave}$ . Otherwise, mouth bars would have been formed and  $N_{dist}^{obs}$  would have been higher. For single-threaded deltas ( $N_{dist}^{obs} = 1$ ) and smooth shorelines, we measured the delta flank angles relative to a reference shoreline to quantify the observed wave flux,  $Q_{w,net}^{obs}$  (Figure 5d). In Equation 14,  $\theta_{right}^{obs}$  and  $\theta_{left}^{obs}$  are the observed right and left delta flank angles with respect to the reference shoreline orientation and  $Q_{w,net}(\theta)$  is the net alongshore sediment transport for an observed angle  $\theta$ .

As in the predictions, the protrusion angle is the average of flank angles representing how far or close the delta is from the maximum wave transport capacity, reaching the maximum for a protrusion angle of  $\sim 45^\circ$ . These angles give an alongshore transport left of the river mouth as  $Q_{w,net}$  for  $0 < \theta < \frac{\pi}{2}$ , and transport right of the river mouth as  $Q_{w,net}$  for  $-\frac{\pi}{2} < \theta < 0$ . The difference in transport between the left and right flank of the delta should, at equilibrium, be equal to the fluvial sediment flux  $Q_{river}$ . Its comparison with the predicted potential maximum wave flux ( $Q_{wave}^{pred}$ , Equation 4) then indicates the observed river-dominance ratio  $R^{obs}$  (Equation 14).

### 3.3.3. Observed Tide Dominance

Like the relation of shoreline shape to the river-dominance ratio, we can recast the observed channel widening into an observed tide-dominance ratio,  $T^{obs}$ , as (Nienhuis et al., 2018, their Equation 8)

$$T^{obs} = \left( \frac{w_m}{w_u} \right)^{obs} - 1 \Big) Uf, \quad (15)$$

where  $w_m$  is a single mouth width ( $w_m = \Sigma_n w_{m,n} / N_{dist}^{0.5}$  for multiple distributaries),  $w_u$  is the fluvial channel width,  $U = \frac{0.5\omega a}{S \cdot u_{river}}$  is the strength of the tidal flow relative to the fluvial flow (with tidal quantities given above),  $f = 1 + \frac{2S}{ka}$  as given above. Tidal quantities ( $\omega$  and  $a$ ) are determined for the constituent (i.e.,  $M_2$ ,  $S_2$ ,  $N_2$ ,  $K_1$ , or  $O_1$ ) with the largest amplitude  $a$ , corresponding to the long-term average tidal amplitude. Fluvial flow is represented by  $u_{river} = Q_{w,river} \beta / w_u^2$ , with  $\beta = \frac{w_u}{d_u}$ , and  $d_u = 0.6 \cdot Q_{w,river}^{1/3}$  (Mikhailov, 1970, Eq. 21). Note that  $Q_{w,river}$  is the fluvial water discharge (in  $m^3 s^{-1}$ ), contrary to the sediment load given by  $Q_{river}$  ( $kg s^{-1}$ ).

### 3.3.4. Sediment Fluxes From Morphology

We place the observed morphology into ternary space to ease visualization and allow a non-dimensional comparison with predictions across morphologic thresholds (cf., an observed river-dominated delta vs. a predicted wave-dominated delta). To do this, we use the observed fluvial sediment flux  $Q_{river}$ , and derive  $Q_{tide}^{obs}$  and  $Q_{wave}^{obs}$ . We quantify the tidal sediment flux based on  $T^{obs}$ , as in  $Q_{tide}^{obs} = T^{obs} \cdot Q_{river}$ . We formulate an observed wave sediment flux  $Q_{wave}^{obs}$  from  $R^{obs}$ , using  $Q_{wave}^{obs} = \frac{Q_{river}}{R^{obs}}$ . We then determine the relative fluxes within the ternary diagram by calculating  $r_x^{obs}$  (Equation 1).

Note that our observed fluxes partially use information from the same underlying global models as the predictions. For example,  $Q_{tide}^{obs}$  is derived from the delta mouth width observations and requires knowledge of the dominant tidal period ( $\omega$ ). An inverse approach without the underlying global models can be taken using assumptions about such parameters (e.g., assuming semi-diurnal tides). This possibility means that two deltas with the same morphology can have different inferred sediment fluxes, or deltas in the same position in the quantitative ternary diagram can have different morphologies.

### 3.3.5. Environmental Conditions From Morphology

Lastly, for completeness, we show how information about the fluvial or marine environment can be deduced in the last step of the observation workflow (Figure 1). This deduction may be helpful in studies where delta morphology can be observed but the environmental conditions cannot (e.g., deducing paleo wave height or paleo tidal range from sedimentary deposits).

If  $Q_{river}$  is known, then wave height information can be inferred, first by estimating  $Q_{wave}$  using Equation 12 or 13, then by estimating  $H_s$  using Equation 8, after assuming a simple distribution of wave energy. Similarly, the tidal amplitude may be inferred from  $Q_{tide}^{obs}$  using Equation 9 (replacing  $Q_{tide}^{pred}$  by  $Q_{tide}^{obs}$  in this instance), if data about along-channel slopes are available. Conversely,  $Q_{river}$  can be inferred from  $T^{obs}$  or  $R^{obs}$  if information is available about  $Q_{tide}$  or  $Q_{wave}$ .

## 3.4. Predictions Versus Observations

We derive two measures of prediction uncertainty. First, we calculate a process uncertainty where we compare predicted and observed wave, tidal, and river influences. We call this uncertainty a ternary error,  $e_{ter}$ ,

$$e_{ter} = \sqrt{\left[ \frac{1}{2} (r_{river}^{pred} - r_{river}^{obs}) + (r_{tide}^{pred} - r_{tide}^{obs}) \right]^2 + \frac{3}{4} [r_{river}^{pred} - r_{river}^{obs}]^2}, \quad (16)$$

defined as the Euclidian distance within the quantitative ternary diagram (in linear scaling) between the observed and predicted process dominance of a delta. This value is based on the cartesian coordinates within the triangle,  $x$  and  $y$ , and their relation to ternary coordinates,  $r_x$ , as  $y = r_{river} \sin 60^\circ = \sqrt{3} r_{river} / 2$  and  $x = r_{tide} + y \cot 60^\circ = r_{tide} + r_{river} / 2$ . The process uncertainty  $e_{ter}$  is 0 for an accurate prediction and 1 for predictions that render an opposite dominance (e.g.,  $r_{river}^{pred} = 1$  but  $r_{river}^{obs} = 0$ , Figure 7).

Second, we do a direct one-to-one comparison of the process and morphologic predictions with observations. We assess the uncertainty using the Median Absolute Error (MAE), which we define as the median of the absolute deviations, for example,  $\text{med} |\theta^{obs} - \theta^{pred}|$  for  $\theta$ . We also compute the Median Relative Error (MRE), which we define as the median of the relative errors, for example,  $\text{med} \left| \frac{\theta^{obs} - \theta^{pred}}{\theta^{obs}} \right|$  for  $\theta$ .



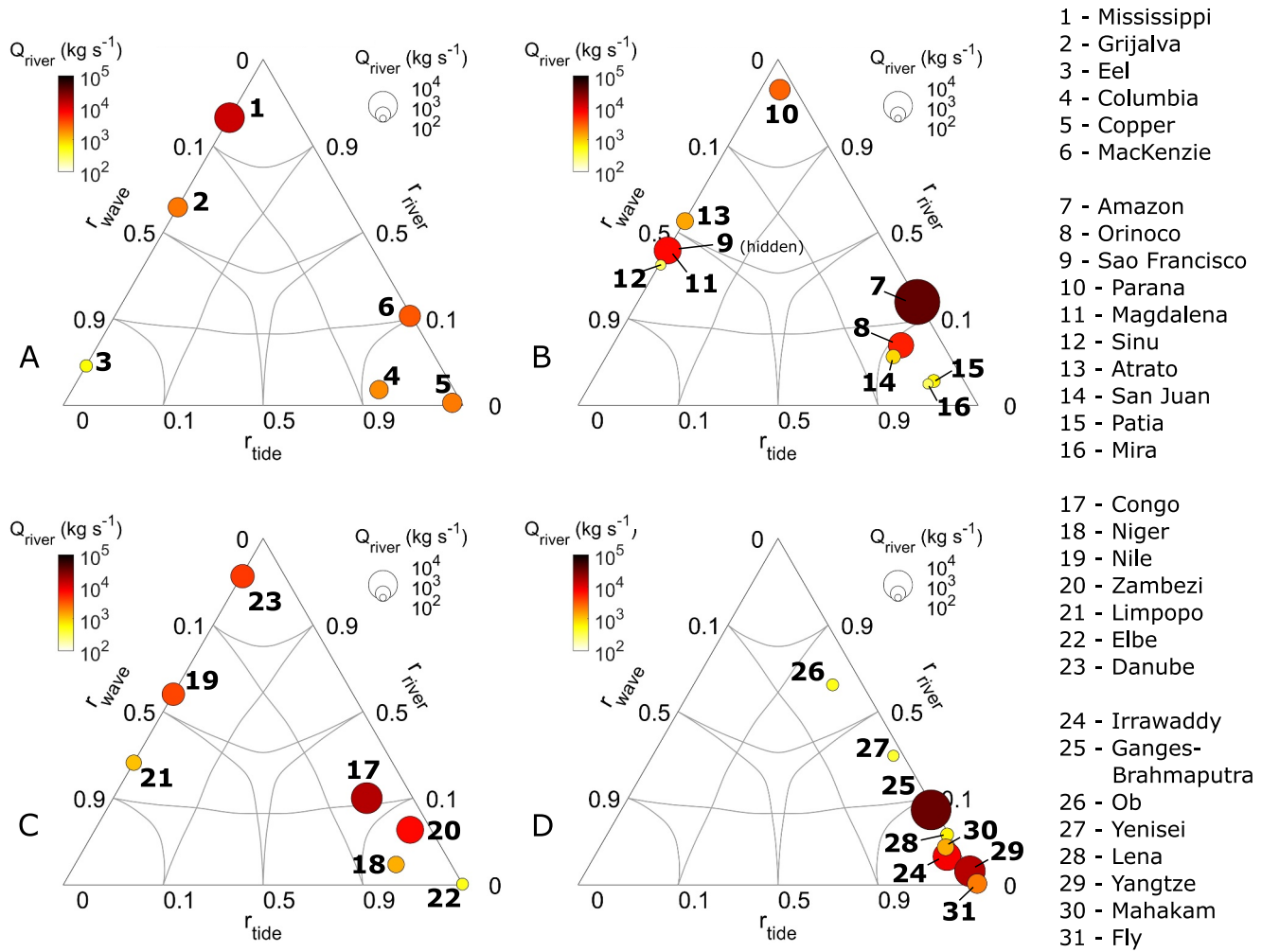


**Figure 8.** Quantitative Galloway ternary diagrams from predicted sediment flux balances for our 31 deltas. We organized deltas in continents such as (a) North America, (b) South America, (c) Africa and Europe, and (d) Asia and Oceania. See Figures 3 and 4 for locations. Axes are in sigmoid scaling (as a “stretching” of axes at the extremes) to help distinguish extreme values.

## 4. Results

### 4.1. Prediction of Delta Morphology

From our 31 deltas, we predict ~23% to be fluvial-dominated (7 out of 31 deltas), ~16% wave-dominated (5 out of 31), and ~61% tide-dominated (19 out of 31), with a broad representation across the ternary space (Figure 8). The predicted morphology varies among deltas, as demonstrated by the number of distributaries (range from 1 to 625 with a median of 4), shoreline protrusion angle (range from  $0.8^\circ$  to  $40^\circ$  with a median of  $10^\circ$ , with 20 out of 31 deltas with undefined protrusion), and channel widening (range from 1 to 860 with a median of 3).

For example, we predict fluvial dominance for the Mississippi ( $r_{\text{River}} = 0.95$ , 20 distributaries) and wave dominance for the Eel ( $r_{\text{Wave}} = 0.97$ , cusate angle of  $0.8^\circ$ ). We predict tidal dominance for the Copper ( $r_{\text{Tide}} \approx 1.0$  and channel widening of 856.3), and fluvial dominance for the Parana ( $r_{\text{River}} = 0.99$  with 172 distributaries). Some deltas have a predicted mixed influence, such as the Atrato ( $r_{\text{River}} = 0.59$  with 2 distributaries,  $r_{\text{Wave}} = 0.41$ ) and the Nile ( $r_{\text{River}} = 0.64$  with 2 distributaries).

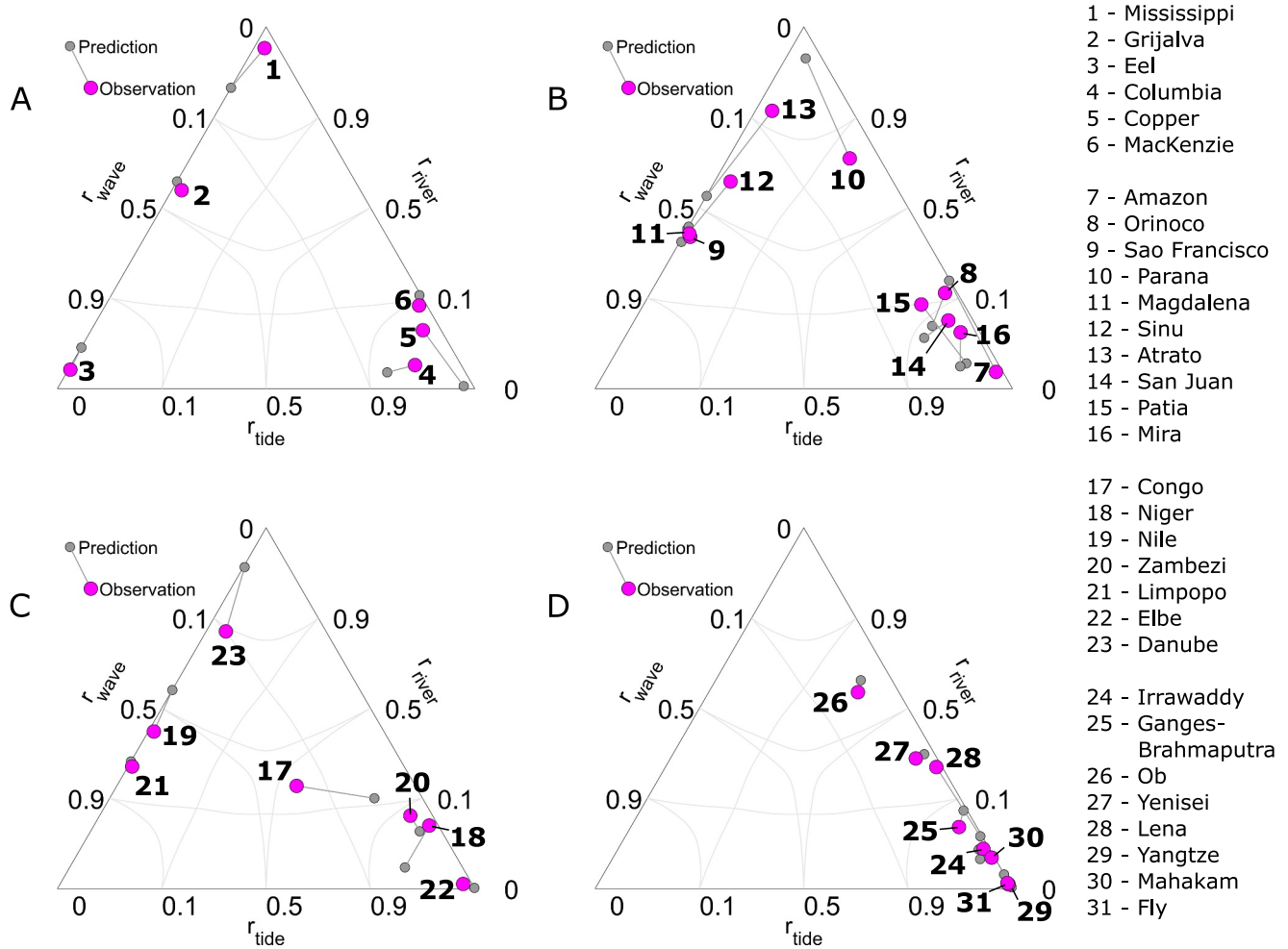


**Figure 9.** Quantitative Galloway ternary diagrams from observation-based fluxes of delta morphology for the selected 31 deltas (magenta dots) compared to the predictions in Figure 8 (gray dots). (a) North America, (b) South America, (c) Africa and Europe, and (d) Asia and Oceania. As in Figure 8, axes are in sigmoid scaling to distinguish among extreme values, so the lines representing error distances are stretched accordingly. However, this scaling does not affect the error calculation.

#### 4.2. Observations of Delta Morphology

In our morphological observations, we find 23% to be fluvial-dominated (7 out of 31 deltas), 16% wave-dominated (5 out of 31), and 61% tide-dominated (19 out of 31). The skew toward tide dominance compared to global deltas (where most deltas are wave-dominated, Nienhuis et al., 2020) is likely because we selected mostly large deltas. We observe fluvial dominance for the Mississippi ( $r_{\text{River}}^{\text{obs}} = 0.99$ , 219 distributaries) and Atrato ( $r_{\text{River}}^{\text{obs}} = 0.93$  with 14 distributaries). Other deltas, such as the Sao Francisco ( $r_{\text{Wave}}^{\text{obs}} = 0.70$  with protrusion angle  $19.8^\circ$ ) and the Magdalena ( $r_{\text{Wave}}^{\text{obs}} = 0.68$  with a protrusion angle of  $30.8^\circ$ ) are observed as wave-dominated (Figure 9).

#### 4.3. Process Predictions Versus Observations

Comparing predictions and observations, we find that errors ( $e_{\text{ter}}$ ) are typically  $<0.20$  (28 out of 31 deltas), with a maximum of  $\sim 0.49$  (Sinu delta) and a minimum of 0.002 (Fly delta) (Figure 10). The median error is 0.04, with a standard deviation of 0.11. From the three deltas with  $e_{\text{ter}} > 0.20$ , the largest errors correspond to river-dominated deltas. Overall, tide-dominated deltas exhibit errors  $<0.20$  (all 19 deltas), with 15 deltas with errors  $<0.05$ . However, other fluvial- and wave-dominated deltas also exhibit errors close to 0 (e.g., Eel, Limpopo, and Ob). Categorically, we find that 29 out of the 31 deltas are classified correctly (i.e., predicted and observed as the same dominance).

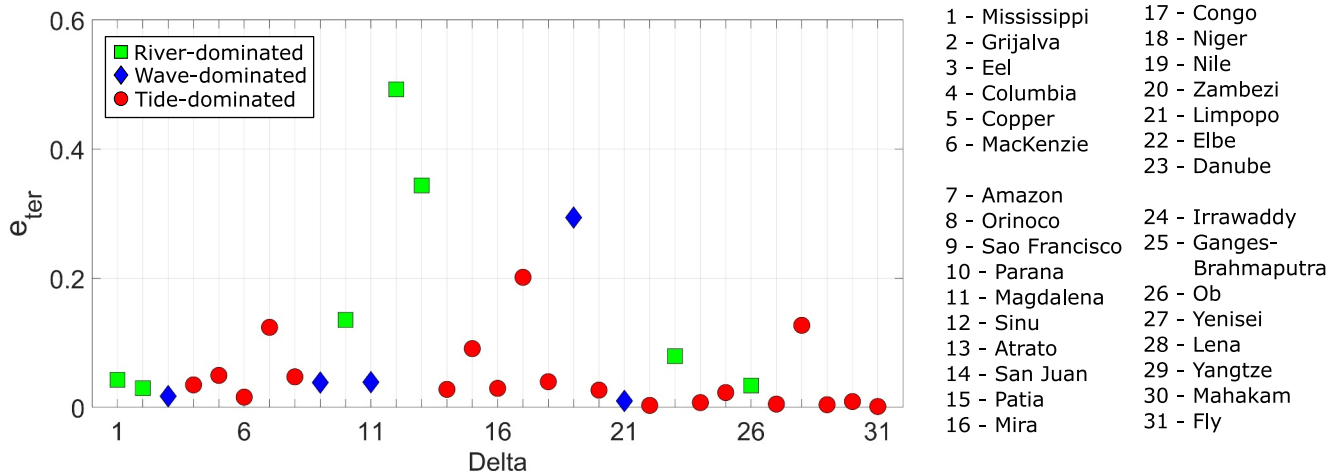


**Figure 10.** Ternary error in predictions,  $e_{ter}$ , with observed dominance indicated by symbols (fluvial: green squares, wave: blue diamonds, tide: red circles).

We find that there is no strong bias in our predictions for the fluvial dominance ratio ( $R^{obs} < R^{pred}$  for 16 deltas, and  $R^{obs} > R^{pred}$  for 15 deltas). However, the uncertainty for individual deltas is considerable, with MAE = 13 and MRE = 91%. The scatter also appears when comparing predicted and observed wave fluxes (MAE of  $820 \text{ kg s}^{-1}$ , and MRE 91%, Figure 11c).

We find a bias in the tide dominance (Figures 11 and 12), which tends to be underpredicted for wave- and river-dominated deltas ( $T^{obs} < 1$ ) and overpredicted for tide-dominated deltas ( $T^{obs} > 1$ ) (Figures 11b and 12). This bias could be from the geometric estimation of the tidal intrusion length (based on the delta slope, assuming no dissipation and an infinite tidal wavelength), which is underestimated for small, steep deltas (where tides protrude upslope) and likely overestimated for larger deltas. The MAE and MRE for  $T$  are similar to those for  $R$ , at 6% and 98%, respectively. Sources of error differ between river-, tide-, and wave-dominated deltas. Wave- and river-dominated deltas have relatively large errors in the predicted tidal influence, whereas errors in tide-dominated deltas are primarily in the estimated river dominance ratio (Figure 12).

#### 4.4. Morphology Predictions Versus Observations

Morphologic prediction errors are more significant than process errors (Figure 13). For the number of distributary channels, there are 6 deltas with 1 predicted and observed distributary channel, 13 deltas where the number of channels is overpredicted, and 12 where it is underpredicted. The median absolute error (MAE) for the number of distributary channels is 12, and the median relative error (MRE) is 85% of the observed channel count. This significant error appears from including extreme predictions that bias the statistics, for example, 340 distributaries for the MacKenzie, 625 for the Amazon, and 146 for the Yangtze (Chang Jiang). We link this limitation to the combination of the relatively low capacity for predicting  $Q_{wave}$  (Figure 11c) and the theoretical assumption that deltas keep bifurcating until  $Q_{river} < N_{dist} \cdot Q_{wave}$ , which ignores the effects of tides and of time. This limitation is also visible in our low capacity for predicting  $R$  (Figure 11a).

There is a bias in the protrusion angles, which are primarily underpredicted (18 deltas) and overpredicted for 2 deltas (Figure 13b). There is a MAE of  $4.1^\circ$  and a MRE of 45%. There are more accurate predictions for channel widening (MAE of 1.2, MRE 25% of the observed widening), but some outliers remain. Several deltas are predicted to have extreme widening, for example, 856.3 for the Copper, 410.8 for the Elbe, and 245.1 for the Fly.

### 5. Discussion

This work compares delta morphology predictions and observations for 31 selected deltas using a novel methodology that expands on the quantitative Galloway ternary diagram. In general, our ternary predictions closely follow the observations, with a median ternary error of 0.02 and a standard deviation of 0.11. We found that most of our tide-dominated deltas exhibited the smallest error. Mixed-influenced deltas were more challenging to predict (maximum error of 0.49). There was also greater uncertainty about delta morphological metrics, with the

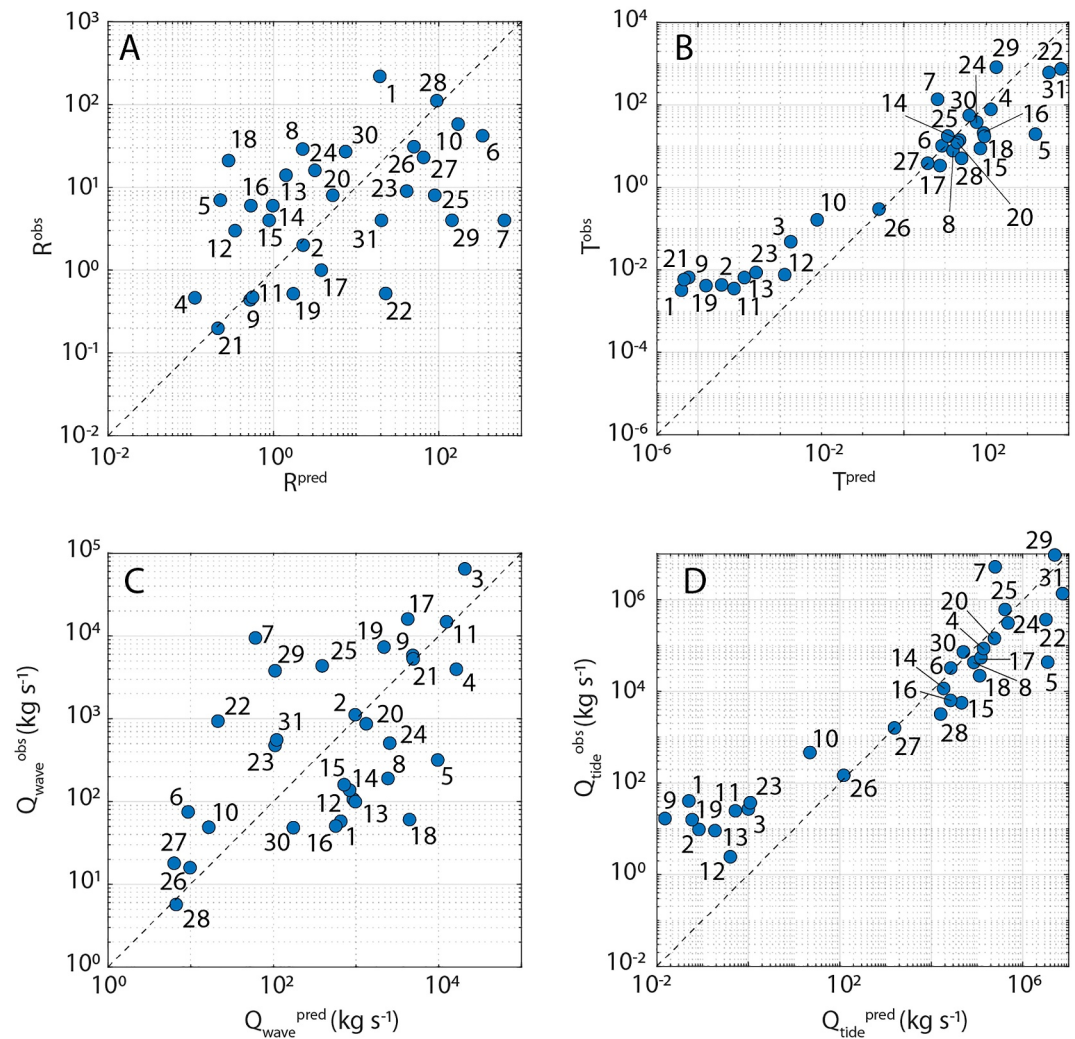


**Figure 11.** Comparison of process predictions and observations for the 31 deltas. (a) Fluvial dominance factor. (b) Tide dominance factor. (c)  $Q_{wave}$ . (d)  $Q_{tide}$ . Numbers refer to deltas in Figure 3.

number of distributary channels estimated within a factor of 3. We now analyze some examples of morphology prediction and observation, including sources of uncertainty and the effects of human interventions.

### 5.1. Sources of Error

There are three sources of prediction error: (a) data for predictions, (b) morphological observations, and (c) assumptions behind the theoretical models. First, regarding data for predictions, riverine fluxes from WBMSed (Cohen et al., 2014) include an average error of  $\sim 34\%$ . Data from other  $Q_{river}$  compilations (Overeem et al., 2022; Syvitski & Saito, 2007) are likely more accurate. In comparison, errors from models of waves (WAVEWATCH III, Chawla et al., 2013) and tides (TPXO, Egbert & Erofeeva, 2002) could be considered negligible. WAVEWATCH III reports a wave height RMS misfit of  $\sim 0.5$  m and an  $R^2$  of 0.92 (Chawla et al., 2013). TPXO reports a tidal amplitude RMS of  $\sim 0.05$  m (Egbert & Erofeeva, 2002). However, our assumptions of wave transformation over continental shelves for wind waves and tides are crude and require improvement, especially along complicated coastlines (e.g., canyons, embayments, and muddy coastlines; see also Section 5.2). Although it is not done here, this error can be assessed through comparison with other models and field observations. Prediction data error can be reduced with more accurate measurements or models that reflect the timescale relevant for creating delta morphology (hundreds to thousands of years). Prediction data can also be improved with field observations, for example, by obtaining  $Q_{tide}$  from field hydrodynamic measurements (e.g., Sassi et al., 2013).

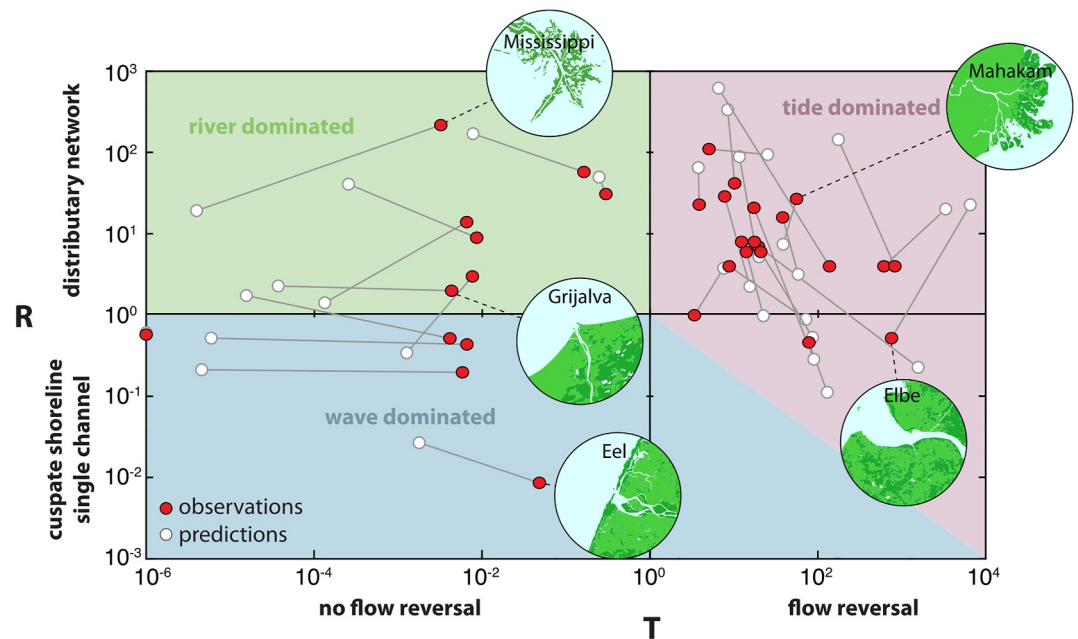


**Figure 12.** Comparison of delta observations and predictions in a cartesian space defined by  $T$  and  $R$ . Numbers refer to deltas in Figure 3.

Second, errors in our morphological observations (number of distributary channels, upstream and mouth channel widths, channel slopes, and flank angles) depend upon the digitizer criteria and precision and are typically in the order of meters according to pixel sizes of the latest Google Earth imagery. Measuring channel slope for tidal flux quantification includes a significant error because of the crude topographic data from the 1 arc-sec SRTM. It can also be challenging to assess active versus inactive distributary channels or to digitize the natural shoreline in complicated wave-dominated deltas (e.g., Magdalena) without including other relevant morphology features, especially those related to the submarine morphology (e.g., shelf depth, prodelta profile, etc.).

Third, a fundamental error stems from our theoretical models for predictions and observations. Predictions are based on the delta apex sediment fluxes, averaged over the past  $\sim 30$  years, even though dominant morphological processes vary spatially within a delta (Broaddus et al., 2022) and vary in time. Our approach also considers a single  $Q_{river}$  value; however, deltas are fed by different grain sizes that respond differently to wave and tidal forcing (Burpee et al., 2015). Enhanced mud supply can also increase bottomset aggradation that aids delta land building (Kim et al., 2022). Sand-mud ratios, therefore, likely affect the relative influence of waves, rivers, or tides.

Our concept of river-to-wave dominance relies on a sediment balance between the river mouth and adjacent shorelines (Nienhuis, Ashton, Nardin, et al., 2016; Nienhuis et al., 2015). This balance may not hold during large floods when sediment escapes beyond the coastal zone (Warrick, 2020) or for all river sediment classes. Also, our method relies on alongshore transport formulations (Ashton & Murray, 2006) that have shortcomings compared to field observations (Cooper & Pilkey, 2004).

Our concept for tide-to-river dominance provides satisfactory results here and elsewhere (Nienhuis et al., 2018), although it simplifies the tidal hydrodynamics that controls sediment transport and land building, especially for deltas with multiple distributaries (Hoitink & Jay, 2016; Nowacki et al., 2015). Tidal predictions may overestimate tidal intrusion for large, low-slope deltas, leading to extreme inferred fluxes in several cases. For example, for the Yangtze,  $Q_{tide}^{obs} = 1.2 \times 10^7 \text{ kg s}^{-1}$  versus a field estimate of  $2 \times 10^5 \text{ kg s}^{-1}$  from Wan et al. (2014). Other high flux estimates, such as  $Q_{tide}^{obs} = 5.2 \times 10^6 \text{ kg s}^{-1}$  for the Amazon and  $Q_{wave}^{obs} = 14 \times 10^3 \text{ kg s}^{-1}$  for the Magdalena could be reasonable, but field data to compare these estimates against is sparse. Tidal observations using channel



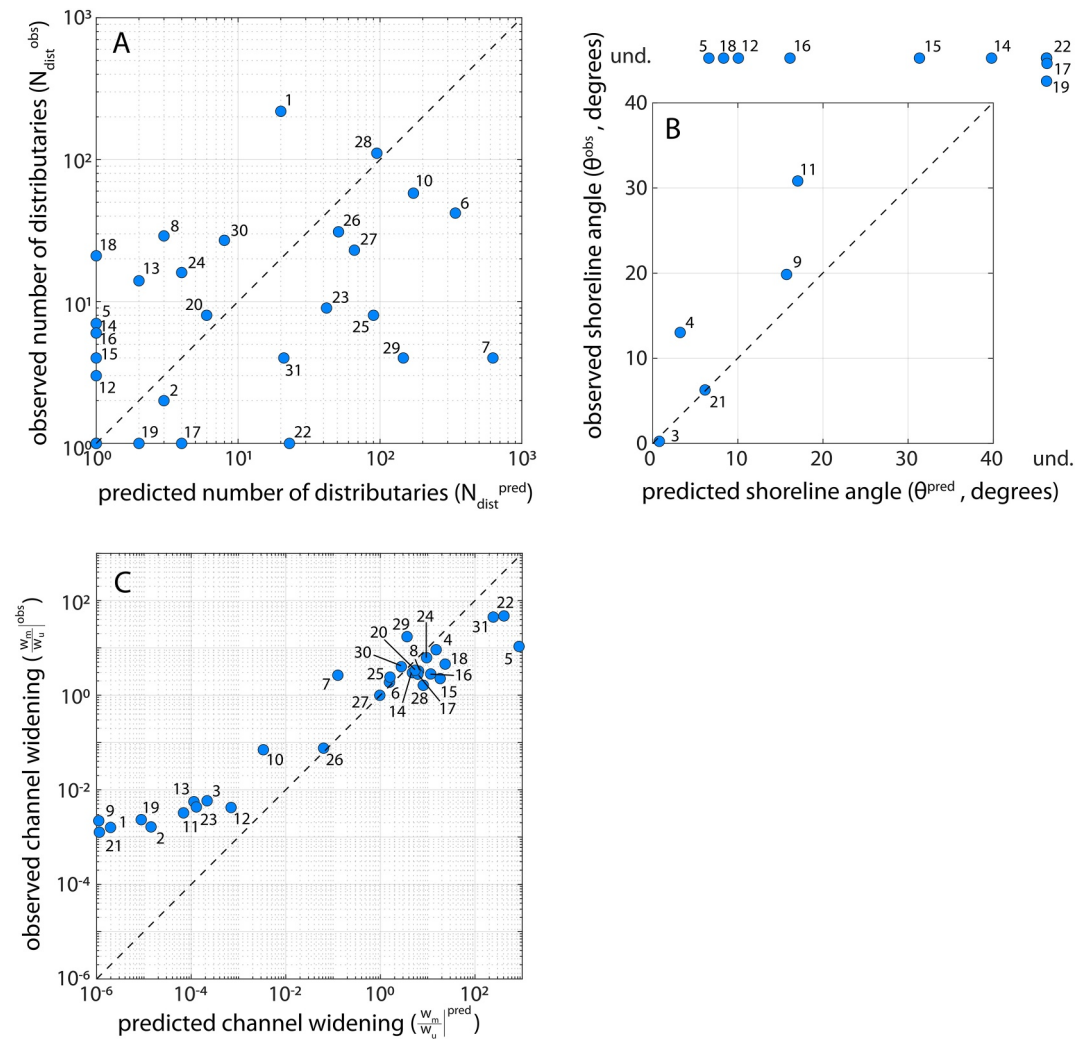


**Figure 13.** Morphologic predictions for the 31 deltas. (a) Number of distributary channels,  $N_{dist}$ . (b) Shoreline angle,  $\theta^{pred}$ , and (c) channel widening,  $w_m/w_u$ . Numbers refer to deltas in Figure 3.

width and channel slope may also overestimate tidal fluxes, for example, in the Lena case, where other processes, such as river ice, may influence morphology (Overeem et al., 2022). Because observations and predictions of tidal fluxes may be overestimated, our analysis could incorrectly suggest a classification with low ternary error.

## 5.2. Disentangling Sources of Error

The three sources of error are difficult to disentangle. Here, we explore potential sources of uncertainty for four deltas by comparing predicted and observed morphological features, that is, number of distributary mouths, cusplate angle, and channel widening (Figure 14 and Table 1).

For the Mississippi (Figure 14a), we underpredicted the number of distributary mouths (20 predicted, 219 observed), which we relate to an overprediction of wave fluxes. This error relates to our theoretical assumption of maximum wave flux capacity at each mouth. In contrast, most mouths are sheltered from the dominant ocean waves and can more easily build mouth bars (Edmonds & Slingerland, 2007). Fluvial sediment flux can also be underpredicted (Cohen et al., 2014).

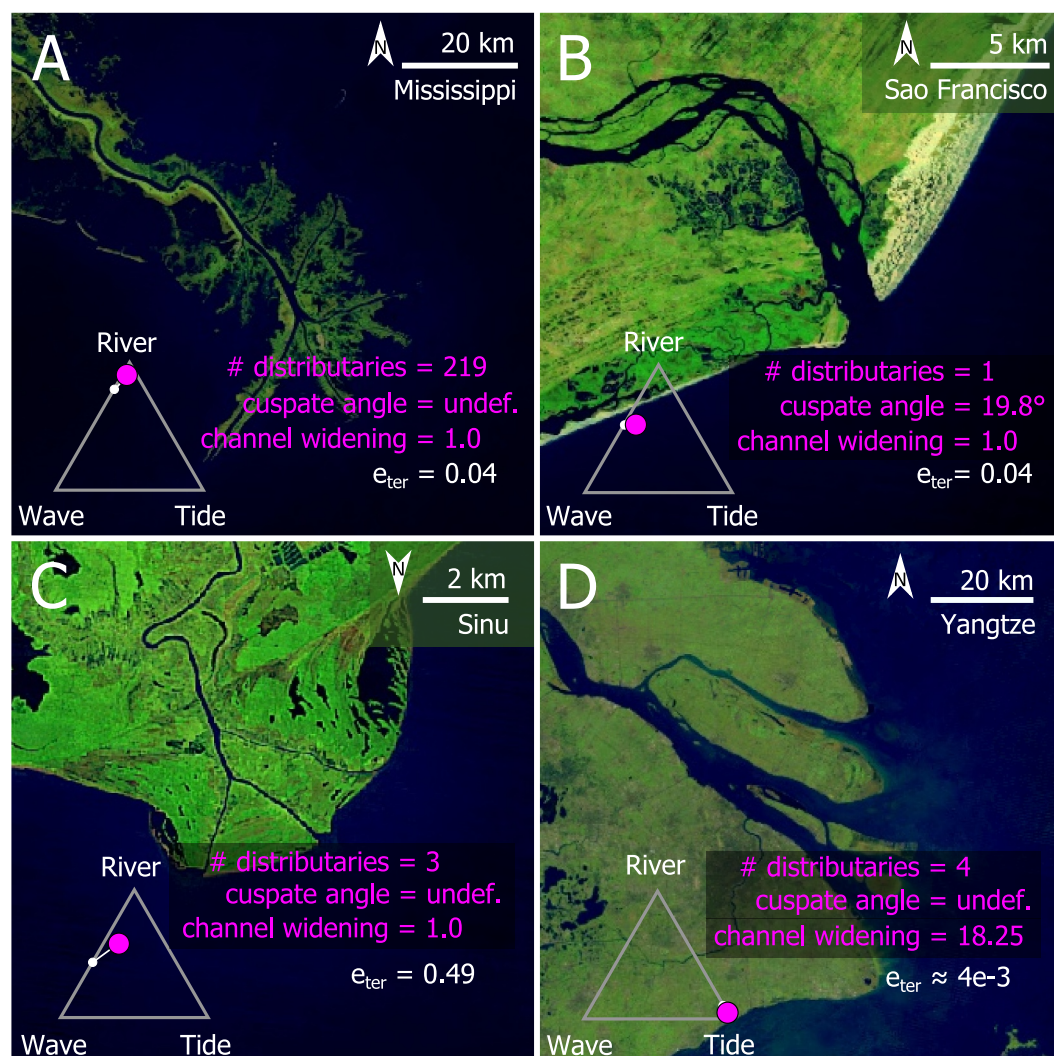


**Figure 14.** Examples of delta morphology prediction (white dot) and observation (magenta dot) within the quantitative ternary diagram, including the observed morphology and ternary error,  $e_{ter}$ . (a) Mississippi, (b) Sao Francisco, (c) Sinu, and (d) Yangtze (Chang Jiang). Imagery from Aquamonitor (<https://aqua-monitor.appspot.com/>).

For the Sao Francisco (Figure 14b), we found similar cusate angles ( $15.7^\circ$  predicted,  $19.8^\circ$  observed). We relate the slight overprediction of wave fluxes to data limitations since no wave data are available close enough to the river mouth. For the Sinu delta (Figure 14c), we predict a relatively small cusate angle ( $10.1^\circ$ ) versus our observation of 3 distributary mouths, which we relate to a similar overprediction of wave fluxes. For the Yangtze (Chang Jiang) (Figure 14d), we overpredict the number of distributaries (146 predicted, 4 observed) and underpredict the channel widening (4.66 predicted, 18.25 observed). We relate these errors to an underprediction of tidal discharge and the oversimplified assumption that mouth bars will form until the river sediment flux per channel decreases below the wave flux.

We can explain the underprediction of wind waves and tides by considering nonlinear transformations over complicated bathymetry without available data. It is known that waves can increase their energy flux onshore of complicated bathymetry, for example, sand shoals and canyons (Bender & Dean, 2005; Bing Wang et al., 2014; Eslami et al., 2019; Paniagua-Arroyave et al., 2019). Conversely, fine sediment dynamics can decrease shoreline wave energy fluxes and tidal amplitudes (Elgar & Raubenheimer, 2008; Winterwerp et al., 2007). These phenomena will likely lead to morphologic prediction errors as we over- or under-predict wave energy fluxes, hence, sediment transport by waves and tides. Our theory also assumes that, for multiple distributary mouths, each outlet

**Table 1**  
*Errors in Predictions and Sources of Uncertainty for the Four Selected Deltas in Figure 14*

Number	Delta	$e_{ter}$	Observed dominance	Prediction/observation comparison—Fluxes prediction	Most prominent potential source of error—Explanation	Particularities
1	Mississippi	0.043	River	Predicted fewer distributary mouths—Overprediction of wave fluxes	Theoretical—Assumption of maximum wave transport capacity at each mouth of multi-channel deltas	Channel diversions, levees, and significant subsidence (Törnqvist et al., 2008; K. Xu et al., 2019; Zhang et al., 2022)
9	Sao Francisco	0.039	Wave	Predicted smaller cuscate angle—Underprediction of wave fluxes	Data—Wind-wave dissipation and scattering over continental shelves	Strandplain with significant inactive and active dune fields (Barbosa & Dominguez, 2004; Dominguez, 1996)
12	Sinu	0.493	River	Predicted fewer distributary mouths and smaller cuscate angle—Overprediction of wave fluxes	Data—Wind-wave dissipation and scattering over continental shelves	Muddy coast, upstream water diversions (Piccardi et al., 2020; Serrano Suarez, 2004)
29	Yangtze (Chang Jiang)	0.004	Tide	Predicted more distributary mouths and smaller channel widening—Underprediction of wave and tidal fluxes	Theoretical—Assumption of continuous mouth bar creation and channel formation	Upstream basin degradation, delta land reclamation, and shoreline embankment (Saito et al., 2001; Wang et al., 2011; Zhang et al., 2022)

would carry the same amount of fluvial sediment, which does not reflect nature (Bolla Pittaluga et al., 2015). Therefore, we assume that waves can move at the maximum capacity at each mouth, which can overestimate the total sediment flux at the delta.

### 5.3. Application of the Quantitative Galloway Ternary Diagram

We foresee three types of applications of the quantitative ternary diagram. First, the morphology predictions can help to project future delta changes under varying boundary conditions. For example, one can predict delta morphology changes in the case of human activities affecting sediment fluxes in the form of increasing loads by, for example, catchment deforestation (J. D. Restrepo et al., 2015) or decreasing loads by, for example, damming (Vörösmarty et al., 2003). These predictions can also be used to hindcast past changes, for example, when reconstructing the historical development of deltas under past environmental change (Nienhuis et al., 2017). In terms of morphology, such sediment load changes will likely have the most considerable effect if they lead to changes in process dominance. A decrease in sediment load can make deltas transition from river- to wave-dominated: wave-driven sediment transport will silt in delta channels, reducing their number, and smooth its shoreline into a cusped shape. A transition to tide dominance will lead to tide-driven sediment import into the river mouth, narrowing channel width preferentially upstream (thereby increasing the relative  $w_m/w_u$ ).

A second application of the ternary diagram is to use predictions (from boundary conditions) or observations (from morphology) to infer sediment and water fluxes. For example, one can estimate the channel-forming tidal sediment discharge amplitude by measuring delta channel widths or shoreline shapes. Such sediment fluxes can be challenging to measure directly (Mei et al., 2021).

A third application is to use morphologic observations to infer (paleo) environmental conditions, such as wave height, river sediment flux, or tidal range (see also Section 3.3.5). These reconstructions are often based on bedforms that indicate paleo-tidal currents or wave-orbital velocity (Willis et al., 1999). The ternary approach can be complementary and provide whole-delta morphology reconstructions (Bhattacharya & Giosan, 2003).

### 5.4. Example Application of the Magdalena Delta

The Magdalena delta (delta 11, Figure 15) is located on the threshold between fluvial and wave dominance. We observe one distributary mouth, a cusped angle of  $30.8^\circ$  and no channel widening ( $R^{obs} = 0.47$ ;  $T^{obs} = 0$ ). Our predictions are similar, that is, 1 distributary, cusped angle of  $17^\circ$ , and no channel widening ( $R = 0.56$ ,  $T = 0$ ) (Figure 15a). At first, our method was successful in prognosing this delta, with a ternary error of  $\sim 0.04$ . However, modern delta morphology is controlled by hard engineering structures that stabilize the mouth channel width (Figure 15b).

Historical maps from 1843 (Martinez et al., 1990) show a single distributary mouth with alongshore extending spits and a general westward orientation (Figure 15c). This morphology suggests wave dominance with a shoreline deflection that indicates sediment bypassing and wave climate control (Nienhuis, Ashton, Nardin, et al., 2016). The historical Magdalena is similar to our predictions: 1 distributary,  $17^\circ$  of cusped angle, and no channel widening, resembling the smaller, nearby Buritaca delta in Colombia ( $11.264056^\circ\text{N}$ ,  $73.770227^\circ\text{W}$ ).

The modern observed Magdalena has steeper delta shoreline angles, that is,  $31.3^\circ$  (left) and  $-30.4^\circ$  (right), but this does not imply that the modern  $Q_{river}$  is greater. Instead, Magdalena's modern morphology relies on human structures that concentrate the flow, which then gets routed to a nearby submarine canyon and would likely limit the nearshore availability of river sediments (Naranjo-Vesga et al., 2022). Steeper delta angles arise, in this case, from limited alongshore sediment bypassing. On the one hand, the human influence on delta morphology prevents an adequate characterization of the Magdalena delta using our quantified Galloway approach. On the other hand, the contrast between what is expected from boundary conditions (our predictions) and what is observed from modern morphology provides a physical framework to explore deviations in sediment fluxes and sediment transport pathways (J. C. Restrepo et al., 2020).

### 5.5. Limitations

There are limitations to the ternary approach. For one, its morphology characterization is limited to the planform shoreline shape. Models for delta elevation change, whether subaerial or subaqueous, should be strongly linked but are often uncoupled in practice (Blum & Roberts, 2009; Nienhuis & van de Wal, 2021; Swenson et al., 2005).



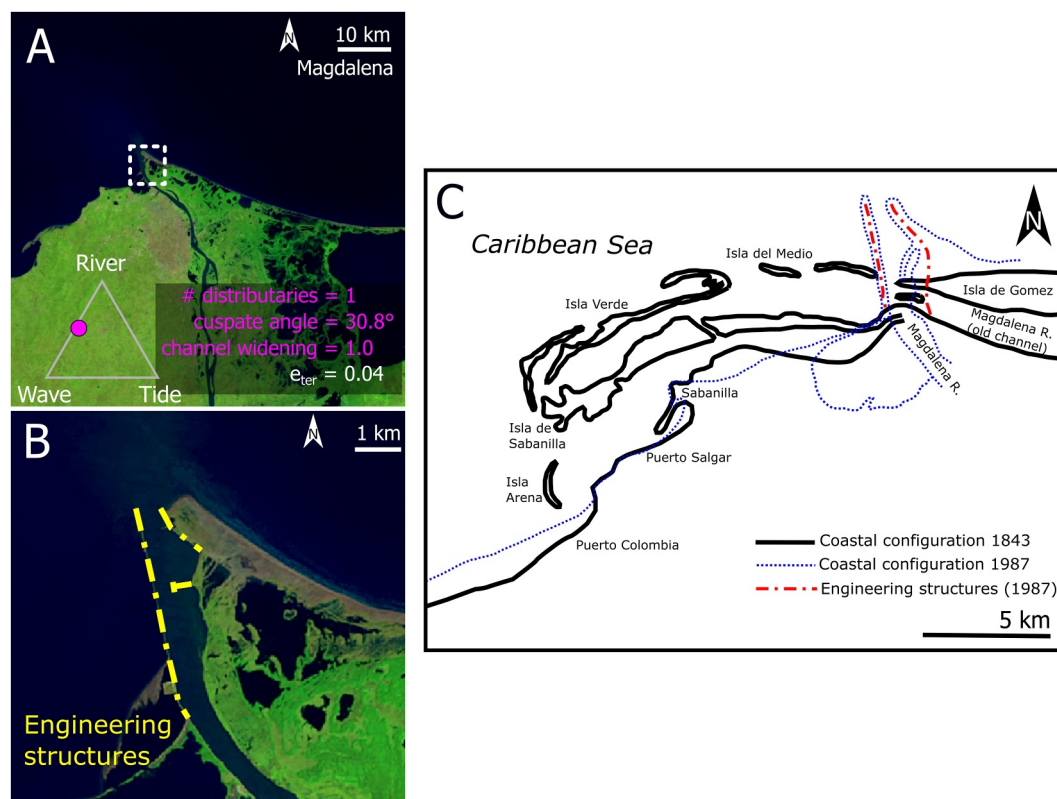


**Figure 15.** An example of the effects of hard engineering structures in delta morphology and their representation within the quantitative Galloway triangle. (a) Magdalena delta at Bocas de Ceniza (near Barranquilla city) in 2022, with a white box showing the close-up in panel (b). Imagery from Aquamonitor. (b) Close up to the Magdalena River mouth, showing current hard structures at mouth flanks (yellow lines). (c) Historical delta morphology changes (1843 and 1887) as given by Martínez et al. (1990, their Figure 2).

Full morphodynamic models like Delft3D could offer a way forward (Broaddus et al., 2022). A promising direction in this case is to use the ternary approach to calibrate and validate Delft3D outcomes against natural examples (Broaddus et al., 2022) and then study its predictions for the evolution of subaerial and subaqueous delta elevation, which are more challenging to test.

Time rates of change pose another challenge for the ternary approach, as ternary predictions assume equilibrium. The ternary approach can be used to indicate a direction of change but not (yet) a rate. Even in the case of directions of change, it will miss delta-shaping events such as avulsions (Prasojó et al., 2022) by providing the overall response of the delta shoreline morphology to a subsequent change in sediment load to the river mouth.

Lastly, the ternary approach is based on a flux balance but does not include a mass balance. Increasing wave influence, for example, with wave smoothening of the shoreline and a reduction in the shoreline angle, will likely lead to erosion near the river mouth and potential deposition further away along the delta flanks (Zăinescu et al., 2024). However, whether this is accompanied by reduced delta area growth and whether sediment composition (sand vs. mud) matters remains unaddressed by the ternary approach.

## 6. Conclusions

We propose a novel method to predict river delta morphology from river, wave, and tidal fluxes and to infer fluxes from morphology observations. The method allows us to compare various sources of morphological uncertainties in a non-dimensional framework. The application of our method to a selection of 31 deltas globally resulted in a median error of 4% (with an 11% standard deviation) with no strong bias toward one of the three dominant delta morphologies. Median absolute errors for delta morphologic characteristics are more significant, with errors for the shoreline angle (4°), downstream widening of delta channels (1.23), and the number of distributary channels



(12). We estimate that the inaccurate calculation of wave and tidal fluxes is the largest source of uncertainty for delta morphology predictions compared with fluvial sediment supply. As our approach predicts first-order delta morphology from sediment fluxes, it offers a way of forecasting how delta morphology will adjust to variations in sediment flux balances, with potential worldwide applications for deltas under climate and global change stressors.

## Data Availability Statement

The data on which this article is based are available in Paniagua-Arroyave and Nienhuis (2024).

## Acknowledgments

This research was supported by the U. S. National Science Foundation (award EAR-1810855) and NWO (VI.Veni.192.123) to JHN, and EAFIT University (award 952-000015) to JFP-A. We thank J.D. Restrepo-Ángel, A. Ashton, A. Valle-Levinson, A.J.F. Hoitink, Y. Saito, L. Velasquez-Montoya, O. Álvarez-Silva, E. Ramos-Chavarriaga, A. Amaya-Saldrarriaga, J. Vargas-Londoño, J.L. Restrepo-Muñoz, D.A. Arboleda-Girón, A.L. Cuervo-Cano, and D. Alvira-Reyes for discussions that enriched this research. The authors sincerely thank Amy East, John B. Shaw, and four anonymous reviewers for their efforts in reviewing and commenting on our manuscript. This work is a contribution to IGCP Project 725 "Forecasting Coastal Change".

## References

- Alcántara-Carrió, J., Caicedo, A., Hernández, J. C., Jaramillo-Vélez, A., & Manzolli, R. P. (2019). Sediment bypassing from the new human-induced lobe to the ancient lobe of the Turbo Delta (Gulf of Urabá, Southern Caribbean Sea). *Journal of Coastal Research*, 35(1), 196–209. <https://doi.org/10.2112/JCOASTRES-D-17-00221.1>
- Anthony, E. J. (2015). Wave influence in the construction, shaping and destruction of river deltas: A review. *Marine Geology*, 361, 53–78. <https://doi.org/10.1016/j.margeo.2014.12.004>
- Ashton, A. D., & Giosan, L. (2011). Wave-angle control of delta evolution. *Geophysical Research Letters*, 38(13), 1–6. <https://doi.org/10.1029/2011GL047630>
- Ashton, A. D., & Murray, A. B. (2006). High-angle wave instability and emergent shoreline shapes: 1. Modeling of sand waves, flying spits, and capes. *Journal of Geophysical Research*, 111(4), 1–19. <https://doi.org/10.1029/2005JF000422>
- Barbosa, L. M., & Dominguez, J. M. L. (2004). Coastal dune fields at the São Francisco River strandplain, northeastern Brazil: Morphology and environmental controls. *Earth Surface Processes and Landforms*, 29(4), 443–456. <https://doi.org/10.1002/ESP.1040>
- Baumgardner, S. E. (2016). *Quantifying galloway: Fluvial, tidal and wave influence on experimental and field deltas (Doctoral dissertation)*. University of Minnesota.
- Bender, C. J., & Dean, R. G. (2005). Wave transformation by axisymmetric three-dimensional bathymetric anomalies with gradual transitions in depth. *Coastal Engineering*, 52(4), 331–351. <https://doi.org/10.1016/j.coastaleng.2004.12.005>
- Bentley, S. J., Blum, M. D., Maloney, J., Pond, L., & Paulsell, R. (2016). The Mississippi River source-to-sink system: Perspectives on tectonic, climatic, and anthropogenic influences, Miocene to Anthropocene. *Earth-Science Reviews*, 153, 139–174. <https://doi.org/10.1016/j.earscirev.2015.11.001>
- Best, J. (2019). Anthropogenic stresses on the world's big rivers. *Nature Geoscience*, 12(1), 7–21. <https://doi.org/10.1038/s41561-018-0262-x>
- Bhattacharya, J. P., & Giosan, L. (2003). Wave-influenced deltas: Geomorphological implications for facies reconstruction. *Sedimentology*, 50(1), 187–210. <https://doi.org/10.1046/j.1365-3091.2003.00545.x>
- Bing Wang, Z., Winterwerp, J. C., & He, Q. (2014). Interaction between suspended sediment and tidal amplification in the Guadalquivir Estuary. *Ocean Dynamics*, 64(10), 1487–1498. <https://doi.org/10.1007/s10236-014-0758-x>
- Blum, M. D., & Roberts, H. H. (2009). Drowning of the Mississippi Delta due to insufficient sediment supply and global sea-level rise. *Nature Geoscience*, 2(7), 488–491. <https://doi.org/10.1038/ngeo553>
- Bolla Pittaluga, M., Coco, G., & Kleinans, M. G. (2015). A unified framework for stability of channel bifurcations in gravel and sand fluvial systems. *Geophysical Research Letters*, 42(18), 7521–7536. <https://doi.org/10.1002/2015GL065175>
- Boyd, R., Dalrymple, R., & Zaitlin, B. A. (1992). Classification of clastic coastal depositional environments. *Sedimentary Geology*, 80(3–4), 139–150. [https://doi.org/10.1016/0037-0738\(92\)90037-R](https://doi.org/10.1016/0037-0738(92)90037-R)
- Broadbent, C. M., Vulis, L. M., Nienhuis, J. H., Tejedor, A., Brown, J., Fofoula-Georgiou, E., & Edmonds, D. A. (2022). First-order river delta morphology is explained by the sediment flux balance from rivers, waves, and tides. *Geophysical Research Letters*, 49(22), e2022GL100355. <https://doi.org/10.1029/2022GL100355>
- Brückner, M. Z. M., Schwarz, C., van Dijk, W. M., van Oorschot, M., Douma, H., & Kleinans, M. G. (2019). Salt marsh establishment and eco-engineering effects in dynamic estuaries determined by species growth and mortality. *Journal of Geophysical Research: Earth Surface*, 124(12), 2962–2986. <https://doi.org/10.1029/2019JF005092>
- Burpee, A. P., Slingerland, R. L., Edmonds, D. A., Parsons, D., Best, J., Cederberg, J., et al. (2015). Grain-size controls on the morphology and internal geometry of river-dominated deltas. *Journal of Sedimentary Research*, 85(6), 699–714. <https://doi.org/10.2110/jsr.2015.39>
- Caldwell, R. L., & Edmonds, D. A. (2014). The effects of sediment properties on deltaic processes and morphologies: A numerical modeling study. *Journal of Geophysical Research: Earth Surface*, 119(5), 961–982. <https://doi.org/10.1002/2013JF002965>
- Caldwell, R. L., Edmonds, D. A., Baumgardner, S., Paola, C., Roy, S., & Nienhuis, J. H. (2019). A global delta dataset and the environmental variables that predict delta formation on marine coastlines. *Earth Surface Dynamics*, 7(3), 773–787. <https://doi.org/10.5194/esurf-7-773-2019>
- Chawla, A., Spindler, D. M., & Tolman, H. L. (2013). Validation of a thirty year wave hindcast using the climate forecast system reanalysis winds. *Ocean Modelling*, 70, 189–206. <https://doi.org/10.1016/j.ocemod.2012.07.005>
- Coffey, T. S., & Shaw, J. B. (2017). Congruent bifurcation angles in river delta and tributary channel networks. *Geophysical Research Letters*, 44(22), 11427–11436. <https://doi.org/10.1002/2017GL074873>
- Cohen, S., Kettner, A. J., & Syvitski, J. (2014). Global suspended sediment and water discharge dynamics between 1960 and 2010: Continental trends and intra-basin sensitivity. *Global and Planetary Change*, 115, 44–58. <https://doi.org/10.1016/j.gloplacha.2014.01.011>
- Coleman, J. M., & Wright, L. D. (1975). Modern river deltas: Variability of processes and sand bodies. In M. lou Broussard (Ed.), *Deltas, models for exploration* (pp. 99–150). Houston Geological Society.
- Cooper, J. A. G., & Pilkey, O. H. (2004). Longshore drift: Trapped in an expected universe. *Journal of Sedimentary Research*, 74(5), 599–606. <https://doi.org/10.1306/022204740599>
- Dalrymple, R. W., Zaitlin, B. A., & Boyd, R. (1992). Estuarine facies models: Conceptual basis and stratigraphic implications. *Journal of Sedimentary Petrology*, 62(6), 1130–1146. <https://doi.org/10.1306/D4267A69-2B26-11D7-8648000102C1865D>
- Dan, S., Walstra, D. J. R., Stive, M. J. F., & Panin, N. (2011). Processes controlling the development of a river mouth spit. *Marine Geology*, 280(1–4), 116–129. <https://doi.org/10.1016/j.margeo.2010.12.005>
- Dominguez, J. M. L. (1996). The Sao Francisco strandplain: A paradigm for wave-dominated deltas? In M. de Batist & P. Jacobs (Eds.), *Geology of siliciclastic shelf seas* (Vol. 117, pp. 217–231). Geological Society Special Publication. Retrieved from <https://www.lyellcollection.org>

- Donchyts, G., Baart, F., Winsemius, H., Gorelick, N., Kwadijk, J., & van de Giesen, N. (2016). Earth's surface water change over the past 30 years. *Nature Climate Change*, 6(9), 810–813. <https://doi.org/10.1038/nclimate3111>
- Edmonds, D. A., & Slingerland, R. L. (2007). Mechanics of river mouth bar formation: Implications for the morphodynamics of delta distributary networks. *Journal of Geophysical Research*, 112(F2), F02034. <https://doi.org/10.1029/2006JF000574>
- Edmonds, D. A., & Slingerland, R. L. (2010). Significant effect of sediment cohesion on delta morphology. *Nature Geoscience*, 3(2), 105–109. <https://doi.org/10.1038/ngeo730>
- Egbert, G. D., Bennett, A. F., & Foreman, M. G. G. (1994). TOPEX/POSEIDON tides estimated using a global inverse model. *Journal of Geophysical Research*, 99(C12), 24821–24852. <https://doi.org/10.1029/94JC01894>
- Egbert, G. D., & Erofeeva, S. Y. (2002). Efficient inverse modeling of Barotropic Ocean tides. *Journal of Atmospheric and Oceanic Technology*, 19(2), 183–204. [https://doi.org/10.1175/1520-0426\(2002\)019<0183:EIMOBO>2.0.CO;2](https://doi.org/10.1175/1520-0426(2002)019<0183:EIMOBO>2.0.CO;2)
- Elgar, S., & Raubenheimer, B. (2008). Wave dissipation by muddy seafloors. *Geophysical Research Letters*, 35(7), 1–5. <https://doi.org/10.1029/2008GL033245>
- Eslami, S., Hoekstra, P., Nguyen Trung, N., Ahmed Kantoush, S., van Binh, D., Duc Dung, D., et al. (2019). Tidal amplification and salt intrusion in the Mekong Delta driven by anthropogenic sediment starvation. *Scientific Reports* 2019, 9(1), 1–10. <https://doi.org/10.1038/s41598-019-55018-9>
- Fagherazzi, S., & Overeem, I. (2007). Models of deltaic and inner continental shelf landform evolution. *Annual Review of Earth and Planetary Sciences*, 35(1), 685–715. Retrieved from <https://www.annualreviews.org/full/10.1146/annurev.earth.35.031306.140128#article-denial>
- Federici, B., & Paola, C. (2003). Dynamics of channel bifurcations in noncohesive sediments. *Water Resources Research*, 39(6), 1162. <https://doi.org/10.1029/2002WR001434>
- Fisher, W. L. (1969). Facies characterization of Gulf Coast Basin Delta systems, with some Holocene Analogues. *Gulf Coast Association of Geological Societies Transactions*, 19, 239–261.
- Frings, R. M., & Kleinhans, M. G. (2008). Complex variations in sediment transport at three large river bifurcations during discharge waves in the river Rhine. *Sedimentology*, 55(5), 1145–1171. <https://doi.org/10.1111/j.1365-3091.2007.00940.x>
- Galloway, W. E. (1975). Process framework for describing the morphologic and stratigraphic evolution of deltaic depositional systems. In M. Lou Broussard (Ed.), *Deltas, models for exploration*. Houston Geological Society.
- Gao, S., Wang, Y. P., & Gao, J.-H. (2011). Sediment retention at the Changjiang sub-aqueous delta over a 57 year period, in response to catchment changes. *Estuarine, Coastal and Shelf Science*, 95(1), 29–38. <https://doi.org/10.1016/j.ecss.2011.07.015>
- Gilbert, G. K. (1885). The topographic features of lake shores.
- Giosan, L., Donnelly, J. P., Constantinescu, S., Filip, F., Ovejanu, I., Vespremeanu-Stroe, A., et al. (2006). Young Danube delta documents stable Black Sea level since the middle Holocene: Morphodynamic, paleogeographic, and archaeological implications. *Geology*, 34(9), 757–760. <https://doi.org/10.1130/G22587.1>
- Goodbred, S. L., & Saito, Y. (2012). Tide-dominated deltas. In R. A. Davis & R. W. Dalrymple (Eds.), *Principles of tidal sedimentology* (pp. 129–149). Springer.
- Hoitink, A. J. F., & Jay, D. A. (2016). Tidal river dynamics: Implications for deltas. *Reviews of Geophysics*, 54(1), 240–272. <https://doi.org/10.1002/2015RG000507>
- Hoitink, A. J. F., Nittrouer, J. A., Passalacqua, P., Shaw, J. B., Langendoen, E. J., Huismans, Y., & van Maren, D. S. (2020). Resilience of river deltas in the anthropocene. *Journal of Geophysical Research: Earth Surface*, 125(3), 1–24. <https://doi.org/10.1029/2019JF005201>
- Jerolmack, D. J., & Swenson, J. B. (2007). Scaling relationships and evolution of distributary networks on wave-influenced deltas. *Geophysical Research Letters*, 34(23), L23402. <https://doi.org/10.1029/2007GL031823>
- Jobe, Z. R., Sylvester, Z., Parker, A. O., Howes, N., Slowey, N., & Pirmez, C. (2015). Rapid adjustment of submarine channel architecture to changes in sediment supply. *Journal of Sedimentary Research*, 85(6), 729–756. <https://doi.org/10.2110/jsr.2015.30>
- Ke, W. T., Shaw, J. B., Mahon, R. C., & Cathcart, C. A. (2019). Distributary channel networks as moving boundaries: Causes and morphodynamic effects. *Journal of Geophysical Research: Earth Surface*, 124(7), 1878–1898. <https://doi.org/10.1029/2019JF005084>
- Kim, M., Kim, W., & Nahm, W. H. (2022). The effect of bottomset on fluviodeltaic land-building process: Numerical modelling and physical experiment. *Basin Research*, 34(5), 1763–1780. <https://doi.org/10.1111/bre.12684>
- Kleinhans, M. G., Ferguson, R. I., Lane, S. N., & Hardy, R. J. (2013). Splitting rivers at their seams: Bifurcations and avulsion. *Earth Surface Processes and Landforms*, 38(1), 47–61. <https://doi.org/10.1002/esp.3268>
- Komar, P. D. (1973). Computer models of delta growth due to sediment input from rivers and longshore transport. *Geological Society of America Bulletin*, 84(7), 2217–2226. [https://doi.org/10.1130/0016-7606\(1973\)84<2217:cmogd>2.0.co;2](https://doi.org/10.1130/0016-7606(1973)84<2217:cmogd>2.0.co;2)
- Konkol, A., Schwenk, J., Katifori, E., & Shaw, J. B. (2022). Interplay of river and tidal forcings promotes loops in coastal channel networks. *Geophysical Research Letters*, 49(10), e2022GL098284. <https://doi.org/10.1029/2022GL098284>
- Langbein, W. B. (1963). The hydraulic geometry of a shallow estuary. *Hydrological Sciences Journal*, 8(3), 84–94. <https://doi.org/10.1080/02626666309493340>
- Liu, J. P., Xue, Z., Ross, K., Wang, H. J., Yang, Z. S., Li, A. C., & Gao, S. (2009). Fate of sediments delivered to the sea by Asian large rivers: Long-distance transport and formation of remote alongshore clinothems. *The Sedimentary Record*, 7(4), 4–9. <https://doi.org/10.2110/sedred.2009.4.4>
- Martinez, J. O., Pilkey, O. H., & Neal, W. J. (1990). Rapid formation of large coastal sand bodies after emplacement of Magdalena river jetties, northern Colombia. *Environmental Geology and Water Sciences*, 16(3), 187–194. <https://doi.org/10.1007/BF01706043>
- Mei, X., Dai, Z., Darby, S. E., Zhang, M., Cai, H., Wang, J., & Wei, W. (2021). Landward shifts of the maximum accretion zone in the tidal reach of the Changjiang estuary following construction of the Three Gorges Dam. *Journal of Hydrology*, 592, 125789. <https://doi.org/10.1016/j.jhydrol.2020.125789>
- Mikhailov, V. N. (1970). Hydrologic-morphometric characteristics of delta branches. *Stud. Rep. Hydrol.*, 9, 146–158. Retrieved from [http://iahs.info/redbooks/a090/iahs\\_090\\_0146.pdf](http://iahs.info/redbooks/a090/iahs_090_0146.pdf)
- Naranjo-Vesga, J., Ortiz-Karpf, A., Wood, L., Jobe, Z., Paniagua-Arroyave, J. F., Shumaker, L., et al. (2020). Regional controls in the distribution and morphometry of deep-water gravitational deposits along a convergent tectonic margin. Southern Caribbean of Colombia. *Marine and Petroleum Geology*, 121(April), 104639. <https://doi.org/10.1016/j.marpetgeo.2020.104639>
- Naranjo-Vesga, J., Paniagua-Arroyave, J. F., Ortiz-Karpf, A., Jobe, Z., Wood, L., Galindo, P., et al. (2022). Controls on submarine canyon morphology along a convergent tectonic margin. The Southern Caribbean of Colombia. *Marine and Petroleum Geology*, 137, 105493. <https://doi.org/10.1016/j.marpetgeo.2021.105493>
- Nienhuis, J. H., Ashton, A. D., Edmonds, D. A., Hoitink, A. J. F., Kettner, A. J., Rowland, J. C., & Törnqvist, T. E. (2020). Global-scale human impact on delta morphology has led to net land area gain. *Nature*, 577(7791), 514–518. <https://doi.org/10.1038/s41586-019-1905-9>

- Nienhuis, J. H., Ashton, A. D., Edmonds, D. A., Houtink, A. J. F., Kettner, A. J., Rowland, J. C., & Törnqvist, T. E. (2023). Reply to: Concerns about data linking delta land gain to human action. *Nature*, 614(7947), E26–E28. <https://doi.org/10.1038/s41586-022-05625-w>
- Nienhuis, J. H., Ashton, A. D., & Giosan, L. (2015). What makes a delta wave-dominated? *Geology*, 43(6), 511–514. <https://doi.org/10.1130/G36518.1>
- Nienhuis, J. H., Ashton, A. D., & Giosan, L. (2016). Littoral steering of deltaic channels. *Earth and Planetary Science Letters*, 453, 204–214. <https://doi.org/10.1016/j.epsl.2016.08.018>
- Nienhuis, J. H., Ashton, A. D., Kettner, A. J., & Giosan, L. (2017). Large-scale coastal and fluvial models constrain the late Holocene evolution of the Ebro Delta. *Earth Surface Dynamics*, 5(3), 585–603. <https://doi.org/10.5194/esurf-5-585-2017>
- Nienhuis, J. H., Ashton, A. D., Nardin, W., Fagherazzi, S., & Giosan, L. (2016). Alongshore sediment bypassing as a control on river mouth morphodynamics. *Journal of Geophysical Research: Earth Surface*, 121(4), 664–683. <https://doi.org/10.1002/2015JF003780>
- Nienhuis, J. H., Ton Houtink, A. J. F., & Törnqvist, T. E. (2018). Future change to tide-influenced deltas. *Geophysical Research Letters*, 45(April), 3499–3507. <https://doi.org/10.1029/2018GL077638>
- Nienhuis, J. H., & van de Wal, R. S. W. (2021). Projections of global delta land loss from sea-level rise in the 21st century. *Geophysical Research Letters*, 48(14), e2021GL093368. <https://doi.org/10.1029/2021GL093368>
- Nowacki, D. J., Ogston, A. S., Nittrouer, C. A., Fricke, A. T., & Van, P. D. T. (2015). Sediment dynamics in the lower Mekong River: Transition from tidal river to estuary. *Journal of Geophysical Research: Oceans*, 120(9), 6363–6383. <https://doi.org/10.1002/2015JC010754>
- Olariu, C., & Bhattacharya, J. P. (2006). Terminal distributary channels and delta front architecture of river-dominated delta systems. *Journal of Sedimentary Research*, 76(2), 212–233. <https://doi.org/10.2110/jsr.2006.026>
- Olliver, E. A., Edmonds, D. A., & Shaw, J. B. (2020). Influence of floods, tides, and vegetation on sediment retention in Wax Lake Delta, Louisiana, USA. *Journal of Geophysical Research: Earth Surface*, 125(1), 1–21. <https://doi.org/10.1029/2019JF005316>
- Orton, G. J., & Reading, H. G. (1993). Variability of deltaic processes in terms of sediment supply, with particular emphasis on grain size. *Sedimentology*, 40(3), 475–512. <https://doi.org/10.1111/j.1365-3091.1993.tb01347.x>
- Overeem, I., Nienhuis, J. H., & Piliouras, A. (2022). Ice-dominated arctic deltas. *Nature Reviews Earth & Environment*, 3(4), 225–240. <https://doi.org/10.1038/s43017-022-00268-x>
- Paniagua-Arroyave, J. F., Adams, P. N., Parra, S. M., & Valle-Levinson, A. (2019). Observations of surface-gravity-wave scattering and dissipation by an isolated shoal related to a cusped foreland. *Continental Shelf Research*, 173, 43–55. <https://doi.org/10.1016/j.csr.2018.12.004>
- Paniagua-Arroyave, J. F., & Nienhuis, J. H. (2024). Predictions and observations of delta morphology using the quantitative Galloway triangle [Dataset]. *Mendeley Data*, V3. <https://doi.org/10.17632/j83n7hbst.3>
- Paola, C., Twilley, R. R., Edmonds, D. A., Kim, W., Mohrig, D., Parker, G., et al. (2011). Natural processes in delta restoration: Application to the Mississippi Delta. *Annual Review of Marine Science*, 3(1), 67–91. <https://doi.org/10.1146/annurev-marine-120709-142856>
- Passalacqua, P., Lanzoni, S., Paola, C., & Rinaldo, A. (2013). Geomorphic signatures of deltaic processes and vegetation: The Ganges-Brahmaputra-Jamuna case study. *Journal of Geophysical Research: Earth Surface*, 118(3), 1838–1849. <https://doi.org/10.1002/jgrf.20128>
- Patruno, S., & Helland-Hansen, W. (2018). Clinoforms and clinoform systems: Review and dynamic classification scheme for shorelines, subaqueous deltas, shelf edges and continental margins. *Earth-Science Reviews*, 185, 202–233. <https://doi.org/10.1016/j.earscirev.2018.05.016>
- Pawlowicz, R. (2020). M\_Map: A mapping package for MATLAB. Retrieved from <https://www.eoas.ubc.ca/~rich/map.html>
- Piccardi, M., Correa, I. D., & Pranzini, E. (2020). Cispata Bay and Mestizos evolution as reconstructed from old documents and maps (16th–20th century). *Journal of Marine Science and Engineering*, 8(9), 1–27. <https://doi.org/10.3390/jmse8090669>
- Postma, G. (1995). Causes of architectural variation in deltas. In M. N. Oti & G. Postma (Eds.), *Geology of deltas* (pp. 3–16). A.A. Balkema.
- Prasojo, O. A., Hoey, T. B., Owen, A., & Williams, R. D. (2022). Slope break and avulsion locations scale consistently in global deltas. *Geophysical Research Letters*, 49(2), e2021GL093656. <https://doi.org/10.1029/2021GL093656>
- Reading, H. G., & Richards, M. (1994). Turbidite systems in deep-water basin margins classified by grain size and feeder system. *American Association of Petroleum Geologists Bulletin*, 78(5), 792–822. <https://doi.org/10.1306/a25fe3bf-171b-11d7-8645000102c1865d>
- Restrepo, J. C., Orejarena-Rondón, A., Consuegra, C., Pérez, J., Llinas, H., Otero, L., & Álvarez, O. (2020). Siltation on a highly regulated estuarine system: The Magdalena River mouth case (Northwestern South America). *Estuarine, Coastal and Shelf Science*, 245, 107020. <https://doi.org/10.1016/j.ecss.2020.107020>
- Restrepo, J. D., Kettner, A. J., & Syvitski, J. (2015). Recent deforestation causes rapid increase in river sediment load in the Colombian Andes. *Anthropocene*, 10, 13–28. <https://doi.org/10.1016/j.ancene.2015.09.001>
- Restrepo, J. D., & López, S. A. (2008). Morphodynamics of the Pacific and Caribbean deltas of Colombia, South America. *Journal of South American Earth Sciences*, 25(1), 1–21. <https://doi.org/10.1016/j.jsames.2007.09.002>
- Rossi, V. M., Kim, W., López, J. L., Edmonds, D., Geleynse, N., Olariu, C., et al. (2016). Impact of tidal currents on delta-channel deepening, stratigraphic architecture, and sediment bypass beyond the shoreline. *Geology*, 44(11), 927–930. <https://doi.org/10.1130/G38334.1>
- Saito, Y., Yang, Z., & Hori, K. (2001). The Huanghe (Yellow River) and Changjiang (Yangtze River) deltas: A review on their characteristics, evolution and sediment discharge during the Holocene. *Geomorphology*, 41(2–3), 219–231. [https://doi.org/10.1016/S0169-555X\(01\)00118-0](https://doi.org/10.1016/S0169-555X(01)00118-0)
- Sassi, M. G., Houtink, A. J. F., de Brye, B., Vermeulen, B., & Deleersnijder, E. (2011). Tidal impact on the division of river discharge over distributary channels in the Mahakam Delta. *Ocean Dynamics*, 61(12), 2211–2228. <https://doi.org/10.1007/s10236-011-0473-9>
- Sassi, M. G., Houtink, A. J. F., Vermeulen, B., & Hidayat, H. (2013). Sediment discharge division at two tidally influenced river bifurcations. *Water Resources Research*, 49(4), 2119–2134. <https://doi.org/10.1002/wrcr.20216>
- Serrano Suarez, B. E. (2004). The Sinú river delta on the northwestern Caribbean coast of Colombia: Bay infilling associated with delta development. *Journal of South American Earth Sciences*, 16(7), 623–631. <https://doi.org/10.1016/j.jsames.2003.10.005>
- Seybold, H., Andrade, J. S., & Hermann, H. J. (2007). Modeling river delta formation. *Proceedings of the National Academy of Sciences of the United States of America*, 104(43), 16804–16809. <https://doi.org/10.1073/pnas.0705265104>
- Shaw, J. B., Mohrig, D., & Whitman, S. K. (2013). The morphology and evolution of channels on the Wax Lake Delta, Louisiana, USA. *Journal of Geophysical Research: Earth Surface*, 118(3), 1562–1584. <https://doi.org/10.1002/jgrf.20123>
- Swenson, J. B., Paola, C., Pratson, L., Voller, V. R., & Murray, A. B. (2005). Fluvial and marine controls on combined subaerial and subaqueous delta progradation: Morphodynamic modeling of compound-clinoform development. *Journal of Geophysical Research*, 110(2), F02013. <https://doi.org/10.1029/2004JF000265>
- Syvitski, J., Anthony, E., Saito, Y., Zăinescu, F., Day, J., Bhattacharya, J. P., & Giosan, L. (2022). Large deltas, small deltas: Toward a more rigorous understanding of coastal marine deltas. *Global and Planetary Change*, 218, 103958. <https://doi.org/10.1016/j.gloplacha.2022.103958>
- Syvitski, J., & Saito, Y. (2007). Morphodynamics of deltas under the influence of humans. *Global and Planetary Change*, 57(3–4), 261–282. <https://doi.org/10.1016/j.gloplacha.2006.12.001>
- Törnqvist, T. E., Wallace, D. J., Storms, J. E. A., Wallinga, J., van Dam, R. L., Blaauw, M., et al. (2008). Mississippi Delta subsidence primarily caused by compaction of Holocene strata. *Nature Geoscience*, 1(3), 173–176. <https://doi.org/10.1038/ngeo129>

- Valle-Levinson, A. (2010). Definition and classification of estuaries. In A. Valle-Levinson (Ed.), *Contemporary issues in estuarine physics* (pp. 1–11). Cambridge University Press.
- Vörösmarty, C. J., Meybeck, M., Fekete, B., Sharma, K., Green, P., & Syvitski, J. P. M. (2003). Anthropogenic sediment retention: Major global impact from registered river impoundments. *Global and Planetary Change*, 39(1–2), 169–190. [https://doi.org/10.1016/S0921-8181\(03\)00023-7](https://doi.org/10.1016/S0921-8181(03)00023-7)
- Vullis, L., Tejedor, A., Ma, H., Nienhuis, J. H., Broaddus, C. M., Brown, J., et al. (2023). River delta morphotypes emerge from multiscale characterization of shorelines. *Geophysical Research Letters*, 50(7), e2022GL102684. <https://doi.org/10.1029/2022GL102684>
- Wan, Y., Gu, F., Wu, H., & Roelvink, D. (2014). Hydrodynamic evolutions at the Yangtze Estuary from 1998 to 2009. *Applied Ocean Research*, 47, 291–302. <https://doi.org/10.1016/j.apor.2014.06.009>
- Wang, H., Saito, Y., Zhang, Y., Bi, N., Sun, X., & Yang, Z. (2011). Recent changes of sediment flux to the western Pacific Ocean from major rivers in East and Southeast Asia. *Earth-Science Reviews*, 108(1–2), 80–100. <https://doi.org/10.1016/j.earscirev.2011.06.003>
- Warrick, J. A. (2020). Littoral sediment from rivers: Patterns, rates and processes of river mouth morphodynamics. *Frontiers in Earth Science*, 8. <https://doi.org/10.3389/feart.2020.00355>
- Willis, B. J., Bhattacharya, J. P., Gabel, S. L., & White, C. D. (1999). Architecture of a tide-influenced river delta in the Frontier Formation of central Wyoming, USA. *Sedimentology*, 46(4), 667–688. <https://doi.org/10.1046/j.1365-3091.1999.00239.x>
- Winterwerp, J. C., de Graaff, R. F., Groeneweg, J., & Luijendijk, A. P. (2007). Modelling of wave damping at Guyana mud coast. *Coastal Engineering*, 54(3), 249–261. <https://doi.org/10.1016/j.coastaleng.2006.08.012>
- Woodroffe, C. D., Nicholls, R. J., Saito, Y., Chen, Z., & Goodbred, S. L. (2006). Landscape variability and the response of Asian Megadeltas to environmental change. In N. Harvey (Ed.), *Global change and integrated coastal management: The Asia-Pacific Region* (Vol. 10, pp. 277–314). Springer. [https://doi.org/10.1007/1-4020-3628-0\\_10](https://doi.org/10.1007/1-4020-3628-0_10)
- Wright, L. D., & Coleman, J. M. (1971). Effluent expansion and interfacial mixing in the presence of a Salt Wedge, Mississippi River Delta. *Journal of Geophysical Research*, 76(36), 8649–8661. <https://doi.org/10.1029/JC076i036p08649>
- Wright, L. D., & Coleman, J. M. (1972). River delta morphology: Profile, wave climate and the role of the subaqueous. *Science*, 176, 1–4.
- Wright, L. D., & Coleman, J. M. (1973). Variations in morphology of major river deltas as functions on ocean wave and river discharge regimes. *American Association of Petroleum Geologists Bulletin*, 57(2), 370–398.
- Xu, K., Bentley, S. J., Day, J. W., & Freeman, A. M. (2019). A review of sediment diversion in the Mississippi River Deltaic Plain. *Estuarine, Coastal and Shelf Science*, 225, 106241. <https://doi.org/10.1016/j.ecss.2019.05.023>
- Xu, Z., & Plink-Björklund, P. (2023). Quantifying formative processes in river- and tide-dominated deltas for accurate prediction of future change. *Geophysical Research Letters*, 50(20), e2023GL104434. <https://doi.org/10.1029/2023GL104434>
- Zăinescu, F., Anthony, E., Vespremeanu-Stroe, A., Besset, M., & Tătu, F. (2023). Concerns about data linking delta land gain to human action. *Nature*, 614(7947), E20–E25. <https://doi.org/10.1038/s41586-022-05624-x>
- Zăinescu, F., Storms, J. E. A., Vespremeanu-Stroe, A., Van Der Vegt, H., Schuster, M., & Anthony, E. (2024). Wave-influenced delta morphodynamics, long-term sediment bypass and trapping controlled by relative magnitudes of riverine and wave-driven sediment transport. *Geophysical Research Letters*, 51(19), e2024GL111069. <https://doi.org/10.1029/2024GL111069>
- Zhang, W., Xu, Y. J., Guo, L., Lam, N. S. N., Xu, K., Yang, S., et al. (2022). Comparing the Yangtze and Mississippi River Deltas in the light of coupled natural-human dynamics: Lessons learned and implications for management. *Geomorphology*, 399, 108075. <https://doi.org/10.1016/J.GEOMORPH.2021.108075>